International Journal of Nanomedicine

Dovepress
Taylor & Francis Group

Open Access Full Text Article

ORIGINAL RESEARCH

Multifunctional HBc Virus-Like Particles Reprogram Immunosuppressive Macrophages and Potentiate CD8$^+$ T Cell Responses for Enhanced Cancer Immunotherapy

Shuntao Liang[1,*], Xiaoxuan Yin[1,*], Yongjie Chi[2,3,*], Keyue Wang[1,*], Li Ma[4], Zhu Yang[2,3], Xin Xue[5], Shoucheng Wang[2,6], Kai Zhao[6], Lianyan Wang[2,3], Juan Ma[1]

[1]Biomedical Innovation Center, Beijing Shijitan Hospital, Capital Medical University, Beijing, 100038, People's Republic of China; [2]Key Laboratory of Green Process and Engineering, State Key Laboratory of Biochemical Engineering, Institute of Process Engineering, Chinese Academy of Sciences, Beijing, 100190, People's Republic of China; [3]School of Chemical Engineering, University of Chinese Academy of Sciences, Beijing, 100049, People's Republic of China; [4]Department of Gynecology and Obstetrics, China-Japan Friendship Hospital, Capital Medical University, Beijing, 100029, People's Republic of China; [5]Institute of Basic Theory, China Academy of Chinese Medical Sciences, Beijing, 100700, People's Republic of China; [6]Zhejiang International Science and Technology Cooperation Base for Biomass Resources Development and Utilization, Taizhou Key Laboratory of Biomedicine and Advanced Dosage Forms, School of Life Sciences, Taizhou University, Taizhou, Zhejiang, 318000, People's Republic of China

*These authors contributed equally to this work

Correspondence: Juan Ma; Lianyan Wang, Email majuan@mail.ccmu.edu.cn; wanglianyan@ipe.ac.cn

Introduction: Tumor-associated macrophages (TAMs) promote immunosuppression, hindering immune checkpoint blockade and immunotherapy efficacy. To overcome this, we developed a novel multifunctional nanovaccine based on hepatitis B core virus-like particles (HBc VLP) to synergistically remodel the immunosuppressive tumor microenvironment through integrated TAM reprogramming and B7-H3 checkpoint blockade.

Methods: The core VLP co-displayed tumor antigen peptide MAGE-A10 and TAM-targeting peptide M2pep via fusion expression. Immunostimulatory CpG oligodeoxynucleotide 1826 (CpG) was encapsulated within VLP. Anti-B7-H3 antibody (αB7-H3) and polyethylene glycol (PEG) were chemically conjugated to the surface for checkpoint blockade and prolonged circulation, forming CpG@VLP-αB7-H3-PEG.

Results: Structural characterization using transmission electron microscopy and dynamic light scattering confirmed the hollow spherical self-assembly of VLP. Nanovaccines efficiently targeted TAMs in vitro and in vivo. Following CpG encapsulation (5.60 μg/mg), the nanovaccine reprogrammed M2-like TAMs into an M1-like phenotype. This was achieved by elevating the M1/M2 ratios of CD86/CD206 and MHC II/CD206 to 15.50-fold and 3.11-fold, respectively, as determined by flow cytometry. Further conjugation of αB7-H3 (250 μg/mg) significantly enhanced T-cell activation in TAM-T cell co-culture assays. In B16-F10 melanoma-bearing mice, reprogrammed iNOS$^+$ M1-like macrophages triggered robust antitumor immunity, achieving a tumor inhibition rate of 63.47%. These macrophages also function as antigen-presenting cells and increase the proportion of tumor-infiltrating Granzyme B$^+$CD8$^+$ T cells. αB7-H3 conjugation further boosted infiltrating immune cells, M1-like macrophages, activated CD69$^+$CD4$^+$/CD8$^+$ T cells, and cytotoxic T lymphocytes. PEGylation amplified systemic tumor-specific immunity and increased tumor inhibition by 80.12%.

Conclusion: This HBc VLP-based nanovaccine constitutes a pioneering multifunctional platform designed to overcome TAM-mediated immunosuppression through synergistic integration of three modalities: antigen presentation, TAM phenotype reprogramming, and B7-H3 checkpoint blockade. To the best of our knowledge, this is the first nanovaccine architecture to enable coordinated immunomodulation. Its modular design supports the clinical translation of solid tumors and personalized immunotherapy.

Keywords: nanovaccine, HBc VLP, TAM reprogramming, B7-H3 checkpoint blockade, tumor immune microenvironment

Received: 19 June 2025
Accepted: 16 September 2025
Published: 17 October 2025

Graphical Abstract

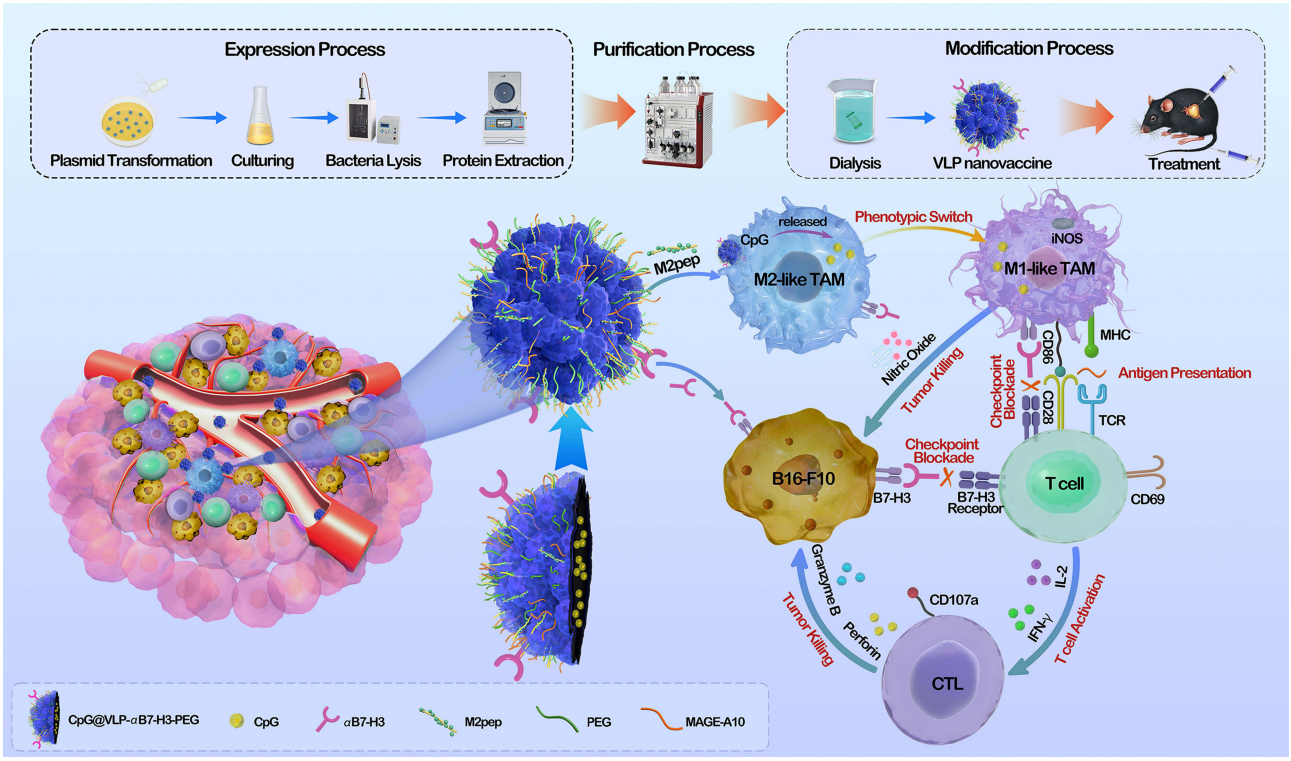

Introduction

Despite significant advances in cancer treatment, it remains a major societal, public health, and economic problem. Global cancer statistics indicate that there are almost 20 million new cases of cancer and approximately 10 million cancer-related deaths by 2022.[1] Therefore, the search for effective antitumor therapies is becoming increasingly important. Cancer immunotherapy has emerged as a promising approach for harnessing the ability of the immune system to recognize and destroy cancer cells.[2,3] However, the efficacy of current immunotherapies, such as immune checkpoint blockade for recovering T cell activity, is often limited by the immunosuppressive tumor microenvironment (TME).[4,5] B7-H3, also known as CD276, is a member of immune checkpoint molecule B7/CD28 family.[6] In contrast to its marginal expression in normal tissues, the B7-H3 protein is significantly expressed in both tumor cells and TME.[7] Moreover, B7-H3 promotes the polarization of pro-tumoral tumor-associated macrophages (TAMs) for tumor progression and immunosuppression.[8,9] Although the receptor for human B7-H3 remains unknown, therapies targeting B7-H3, including antibodies, antibody-drug conjugates, and chimeric antigen receptor T cells, have shown promising results in both preclinical and clinical trials.[10–12]

TAMs are emerging as key regulators of the TME and promising therapeutic targets.[13,14] TAMs, particularly the M2-like phenotype, significantly contribute to the immunosuppressive TME by expressing inhibitory immune checkpoints and secreting anti-inflammatory cytokines.[15] M2-like TAMs are essential for facilitating tumor metastasis and augmenting drug resistance in tumors.[16,17] Moreover, TAMs are plastic and can transform into an M1-like phenotype in response to changes in TME or therapeutic interventions.[18] As professional antigen-presenting cells (APCs) and a bridge between innate and adaptive immunity, M1-like macrophages play a vital role in inducing antitumor immunity by secreting proinflammatory cytokines.[19] Thus, reprogramming M2-like TAMs to an M1-like phenotype holds great promise as a strategy for improving the immunosuppressive TME.[20] One approach to reprogramming M2-like TAMs involves the use of CpG oligodeoxynucleotides, which reprogram M2-like TAMs toward an M1-like phenotype through the Toll-like receptor 9 (TLR9) MyD88-dependent signaling pathway. This process leads to the secretion of several proinflammatory

cytokines, including IL-6, IL-12, and IFN-α, which subsequently activate APCs and T cells.[21,22] However, the systemic administration of CpG oligodeoxynucleotides can trigger cytokine release syndrome and systemic autoimmunity.[23] Therefore, the targeted delivery of CpG oligodeoxynucleotides to M2-like TAMs is highly important for enhancing therapeutic efficacy.

Virus-like particles (VLP) mimic the conformation of the native virus, but do not contain viral nucleic acids and are therefore not infectious.[24] VLP have the advantages of good uniformity, symmetrical macromolecular structure, and nontoxicity and can display antigens and targeted molecules on the capsid surface through chemical conjugation or genetic recombination technology.[25] Among the many VLP, hepatitis B virus core antigen (HBc) VLP provide multiple sites for the insertion of exogenous antigen sequences, such as fusion of exposed immune epitopes and/or cell-targeting signals, while maintaining their self-assembly ability.[26] Moreover, during the assembly process, genetic materials or immunostimulatory sequences can be packaged, inducing strong T-helper 1 (Th1) and cytotoxic T lymphocyte (CTL) effects, which are expected to be effective delivery systems for cancer immunotherapy.[27] Additionally, the biocompatibility and biodegradability of HBc VLP are crucial merits that support their potential application in innovative drug delivery system.[28] Polyethylene glycol (PEG) coating has been widely recognized as a crucial factor for improving the biophysical and chemical properties of nanoparticles.[29] By reducing protein adherence and macrophage removal, PEG enhances the stability and circulation time of nanoparticles.[30]

Melanoma-associated antigen family A (MAGE-A) proteins are expressed in various cancers of different histological origins, including melanoma, lung cancer, prostate cancer, breast cancer, hepatocellular carcinoma, head and neck cancer, and germinal cells.[31,32] MAGE-A proteins are attractive targets for active-specific and adoptive cancer immunotherapies owing to their relatively high tumor specificity. In the present study, based on advantages of HBc VLP,[33] the hepatitis B virus core antigen was modified with two peptides, namely, the TAM-targeting peptide (M2pep) and the MAGE-A10$_{254\text{-}262}$ peptide, and self-assembled into hollow virus-like particles (HBc-M2pep-VLP$_{\text{MAGE-A10,}}$ VLP). M2pep shows a greater binding affinity to M2-like macrophages than to other leukocytes.[34] Compared with other MAGE-A antigens, MAGE-A10 is distinct in its ability to elicit more frequent adaptive immune responses.[35] Subsequently, CpG oligodeoxynucleotide 1826 (CpG) was loaded inside the VLP and a blocking anti-B7-H3 antibody (αB7-H3) was attached to the outside for immune checkpoint blockade. Additionally, a PEG coating was applied to the surface of the CpG@VLP-αB7-H3 nanovaccines, increasing the stability and circulation time of the nanoparticles. The CpG@VLP-αB7-H3-PEG nanovaccine efficiently reprogrammed M2-like TAMs to the M1-like phenotype and enhanced T cell activation and cytotoxicity in B16-F10 melanoma-bearing mice, demonstrating synergistic antitumor effects.

Materials and Methods

Preparation and Characterization of the VLP Nanovaccine

To enable tumor antigen enrichment and TME targeting, MAGE-A10$_{254\text{-}262}$ (GLYDGMEHL) and the M2pep sequence (YEQDPWGVKWWY) were synthesized by GL Biochem Ltd. (Shanghai, China) and inserted into the major immune-dominant region (MIR) and N-terminus of the HBc183 amino acid sequence, respectively; moreover, 6xHis-tag was attached to facilitate protein purification. The C-terminal nucleic acid-binding domain of HBc183 was truncated to HBc149 to load immunostimulatory CpG oligodeoxynucleotide 1826 (CpG). The HBc-M2pep-VLP$_{\text{MAGE-A10}}$ (VLP) sequence was cloned into the pET28a vector using BamHI and HindIII restriction sites. The recombinant plasmid was synthesized by Taihe Biotechnology Co., Ltd. (Beijing, China) and transformed into engineered *Escherichia coli* BL21 (DE3). After culturing in Luria–Bertani (LB) medium, VLP nanovaccines expressed in DE3 cells were obtained from the inclusion bodies. The inclusion body proteins were collected and dissolved in PBS containing 8 M urea and 0.5 mM DTT at 4 °C on a vertical mixer for depolymerization for 4 days. The VLP monomer protein was purified using nickel affinity chromatography (Cytiva) and eluted with PBS containing 300 mM imidazole and 8 M urea. For the Western blot (WB) analysis, a total of 20 μg protein was separated on a 12% SDS-PAGE gel and transferred to a PVDF membrane. After blocking with 5% skimmed milk, the targeted protein was detected with anti-6xHis-tag antibody (1:3000; ab245114, Abcam), followed by HRP-conjugated goat anti-rabbit antibody (1:5000; 1705046, Bio-Rad). After three days of dialysis in PBS, the self-assembled VLP were characterized, and the morphology of the VLP protein was examined using

transmission electron microscopy (JEM1400, JEOL Ltd., Japan). For CpG embedding, 20 nmol CpG oligodeoxynucleotide 1826 (Sangon Bioench, Shanghai, China) was added to 10 mg of VLP protein during dialysis in PBS for 3 days to obtain CpG@VLP (5.60 μg/mg). The average mean hydrodynamic particle size (nm) and zeta potential (mV) of the VLP nanovaccines were measured using a particle size analyzer (Malvern, Cambridge, UK). For αB7-H3 conjugation, 10 mg of CpG@VLP was exposed to Sulfo-SMCC (22322, Thermo Fisher Scientific, USA), and 2.5 mg of αB7-H3 (InVivoMAb MJ18, BioXCell, USA) was exposed to Traut's reagent (26101, Thermo Fisher Scientific). The CpG@VLP-SMCC and αB7-H3-SH samples were immediately mixed after removing the excess crosslinking agent using a 100 kDa ultrafiltration tube and incubated overnight at 4 °C in a vertically oriented suspension. Conjugated CpG@VLP-αB7-H3 was purified by size-exclusion chromatography using Superose 6 Increase 10/300 GL (Cytiva). The specific binding of CpG@VLP-αB7-H3 to B16-F10 tumor cells was examined by flow cytometry (BD FACSCanto II, BD Biosciences, USA) with a FITC-labeled anti-rat IgG secondary antibody (33307ES60, Yeasen Biotechnology, Shanghai) to detect αB7-H3 portion and analyzed with FlowJo software. For PEG coating, mPEG5k-ALD (JenKem Technology Co., Ltd., Beijing) was added to the VLP or CpG@VLP-αB7-H3 nanovaccines at a molar ratio of 10:1 and incubated at 4 °C overnight to obtain VLP-PEG or CpG@VLP-αB7-H3-PEG nanovaccines.

Cellular Viability of Macrophages

Cell viability was assessed using the colorimetric Cell Counting Kit-8 (CCK-8) assay (Dojindo, Japan). Briefly, RAW 264.7 (ATCC TIB-71) cells were plated at 2×10^4 cells/well in 96-well plates containing 100 μL growth medium per well. Subsequently, the macrophages were cocultured with 100 μL of VLP or CpG@VLP at various concentrations for 24 h. Ten microliters of CCK-8 reagent was then added to each well, and the mixture was further incubated with the cells at 37 °C for 4 h. The absorbance was measured at 450 nm and the viability was calculated.

Evaluation of VLP Nanovaccines for TAM Targeting in vitro

To mimic TAMs, RAW264.7 cells were pulsed with the supernatant from B16-F10 melanoma cells for 24 h. The cells were incubated with FITC-labeled VLP, scrambled M2pep sequence (WEDYQWPVYKGW) control (sc) VLP, or VLP-PEG at 37 °C for 4 h. The cells were stained with DAPI, an anti-lysosome mAb (ab108508, Abcam), and a donkey anti-rabbit 594 fluorescent secondary antibody (A32754, Thermo Fisher Scientific). Coverslips were mounted onto glass slides and imaged using a Nikon A1 confocal microscope. Bone marrow-derived macrophages (BMDMs) were generated to quantitatively evaluate the ability of VLP nanovaccines to target TAMs in vitro. Briefly, bone marrow (BM) cells were harvested from the femur and tibia of 6–8-week-old C57BL/6 mice (Beijing Huafukang Bioscience, Beijing, China). BM cells were then cultured in RPMI 1640 medium supplemented with 10 ng/mL macrophage colony-stimulating factor (M-CSF, Thermo Fisher Scientific) for 6 days at 37 °C to harvest immature BMDMs. Immature macrophages were then pulsed for an additional 24 h in fresh medium containing the supernatant from B16-F10 melanoma cells to generate TAMs. Next, the cells were incubated with FITC-labeled VLP, scVLP, or VLP-PEG nanovaccines at 37 °C for 4 h. Finally, the treated cells were washed with PBS to remove excess VLP nanovaccines for flow cytometry analysis, and the percentage of $FITC^+$ cells in each sample was measured using FlowJo software.

Evaluation of VLP Nanovaccines for TAM Targeting in vivo

Subcutaneous tumors were formed by injecting 5×10^5 B16-F10 (ATCC CRL-6475) cells into the dorsum of 8-week-old SCID mice (Beijing Huafukang Bioscience). Tumor-bearing mice were used 2 weeks post-inoculation, with a maximum tumor diameter of 1.5 cm. For intravenous injection, 100 μg of Cy5-labeled VLP (100 μL) was injected into the tumor-bearing mice. At 30 min, mice under isoflurane inhalation anesthesia were sacrificed by cervical dislocation, and the tumors and organs were harvested. The tissues were imaged using IVIS Lumina III and the tumors were fixed overnight with 4% (w/v) paraformaldehyde. The tumors were then cryosectioned, stained with a FITC-labeled anti-F4/80 antibody (BM8, Invitrogen) or anti-CD206 antibody (ab64693, Abcam), stained with DAPI, and imaged using a Leica SP8 STED 3X confocal microscope.

Evaluation of TAM Phenotype Reversion in vitro

TAMs from B16-F10 supernatant-pulsed BMDMs were incubated with CpG, VLP, or CpG@VLP for 24 h. The cells were then collected and pre-incubated with mouse BD Fc Block purified anti-mouse CD16/CD32 mAb 2.4G2. CD11b, F4/80, CD206, CD86, and MHC II TAM markers were identified using flow cytometry to evaluate TAM phase reversion. The following fluorescent antibodies were used: PE-conjugated anti-CD11b (M1/70, Invitrogen), FITC-conjugated anti-F4/80 (BM8, Invitrogen), PerCP-eFluor 710-conjugated anti-CD206 (MR6F3, Invitrogen), PE/Cyanine7-conjugated anti-CD86 (GL1, BD Biosciences) and brilliant violet 421-conjugated anti-MHC II (2G9, BD Biosciences).

Evaluation of T Cell Activation in vitro

TAMs from B16-F10 supernatant-pulsed BMDMs were incubated with CpG@VLP or CpG@VLP-αB7-H3 nanovaccines for 24 hours. The cells were then washed with medium to remove excess VLP nanovaccines. T cells from the spleens of congenic C57BL/6 mice were sorted using the EasySep™ Mouse CD90.2 Positive Selection Kit II (STEMCELL TECHNOLOGIES, Canada). T cells (1×10^5 cells) were then cocultured with CpG@VLP-treated TAMs or CpG@VLP-αB7-H3-treated TAMs at a ratio of 8:1 in the presence of 1 μg/mL anti-CD3e mAb (145–2C11, BD Biosciences) for 72 h in a 96-well round bottom plate. T cell proliferation was detected using a CCK-8 assay, and the levels of IL-2, IFN-γ, IL-4, and IL-17A were determined using a Cytometric Bead Array (CBA) Mouse Th1/Th2/Th17 Cytokine Kit (BD Biosciences) according to the manufacturer's instructions.

Evaluation of the in vivo Antitumor Efficacy of the VLP Nanovaccines

To investigate the antitumor efficacy of the different nanovaccine formulations, 6–8-week-old C57BL/6 mice (Beijing Huafukang Bioscience) were subcutaneously (s.c.) inoculated with 5×10^5 B16-F10 tumor cells. When the average tumor diameter reached approximately 5 mm on day 7, mice were randomly grouped. Mice were administered 300 μL of tribromethanol (12.5 mg/mL) intraperitoneally (i.p.) for anesthesia, and then the mice were intratumorally (i.t.) administered PBS, αB7-H3 (25 μg), CpG@VLP (100 μg), CpG@VLP-αB7-H3 (100 μg), or CpG@VLP-αB7-H3-PEG (100 μg) in a total volume of 100 μL, which was continued every other day. On Day 12, the mice were treated with a triple dose in a total volume of 300 μL via intraperitoneal injection. Relative tumor volume (V) was measured every 2 or 3 days according to the following formula: $V = \text{length} \times (\text{width})^2/2$. All tumors were excised on day 15 after implantation and the tumor inhibition rate (R) was calculated as follows: R = (tumor volume of the control group – tumor volume of the treated group)/tumor volume of the control group × 100%.

Tumor Immune Microenvironment Analysis

On the 15th day after B16-F10 tumor implantation, each mouse was administered i.p. with 300 μL of tribromethanol (12.5 mg/mL) for anesthesia. The mice were sacrificed by cervical dislocation, and the tumors were digested (10 U/mL collagenase I and 400 U/mL collagenase IV in HBSS) to obtain single-cell suspensions and preincubated with 2.4G2. For M1/M2-like TAM analysis, the cells were stained with surface antibodies, including FITC-conjugated anti-CD45 (30-F11, BD Biosciences), Brilliant Violet 605-conjugated anti-CD11b (M1/70, BioLegend), PE-conjugated anti-F4/80 (T45-2342, BD Biosciences), and PerCP-eFluor 710-conjugated anti-CD206, followed by fixation/intracellular buffer (BD Biosciences) and stained with allophycocyanin-conjugated anti-iNOS (W16030C, BioLegend). For T-cell activation analysis, cells were stained with FITC-conjugated anti-CD45, PE/Cyanine7-conjugated anti-CD3 (17A2, BD Biosciences), PE-conjugated anti-CD4 (GK1.5, Invitrogen), allophycocyanin-conjugated anti-CD8a (53–6.7, Invitrogen), and Super Bright 600-conjugated anti-CD69 antibodies (H1.2F3, Invitrogen). For $CD8^+$ T cytotoxicity analysis, the cells were stained with surface antibodies, including FITC-conjugated anti-CD45, PerCP/Cyanine5.5-conjugated anti-CD3 (17A2, BD Biosciences), and Brilliant Violet 605-conjugated anti-CD8a (53–6.7, BD Biosciences), followed by fixation/intracellular buffer and further stained with allophycocyanin-conjugated anti-perforin (S16009B)/Alexa Fluor® 700-conjugated anti-granzyme B (QA16A02) from BioLegend. All antibodies were used according to the manufacturer's instructions and incubated with the cells for 30 min in the dark at 4 °C for flow cytometric analysis.

Systemic Tumor Antigen-Specific Antitumor Immunity Analysis

When the B16-F10 tumor-bearing mice were sacrificed after treatment, their spleens were collected to obtain single-cell suspensions. Splenocytes were restimulated with VLP (5 μg/mL) or cocultured with B16-F10 tumor cells (50:1) in vitro. After 48 h of VLP restimulation, splenocyte proliferation was evaluated using CCK-8 assay. The activation of T cells and cytotoxic T cells was measured by flow cytometry. After pre-incubation with 2.4G2, cells were stained with FITC-conjugated anti-CD3 (145–2c11, Invitrogen), PE/Cyanine7-conjugated anti-CD107a (1D4B, BD Biosciences), allophycocyanin-conjugated anti-CD8a, and Super Bright 600-conjugated anti-CD69 antibodies. Cytokine secretion from the culture supernatant was determined using a CBA Mouse Th1/Th2/Th17 Cytokine Kit via flow cytometric analysis according to the manufacturer's instructions. In vitro-generated splenocytes were cocultured with B16-F10 tumor cells for 72 h, and the secretion of LDH (MAK066, Sigma-Aldrich), granzyme B (ab238265, Abcam), and perforin (NBP3-00452, Novus Biologicals) was determined using a specific ELISA kit according to the manufacturer's instructions.

Tumor Tissue Immunofluorescence Staining

On the 15th day after B16-F10 tumor seeding, tumor tissues were collected and fixed in 4% paraformaldehyde solution. The tumor tissues were embedded in paraffin, sectioned, and stained with DAPI, an anti-CD8 mAb (1:500; 98941S, CST), and an anti-F4/80 mAb (1:5000; ab300421, Abcam) with the assistance of Alpha X Biotech Co., Ltd. (Beijing). After processing, all stained sections were analyzed using an automatic multispectral imaging system and imaging software (ZEN 3.3, ZEISS).

RNA-Seq Analysis

In accordance with the manufacturer's instructions for TRIzol (Ambion), total RNA was extracted from splenocytes or $CD45^+$ cells in tumor tissue using the EasySep™ Mouse TIL (CD45) Positive Selection Kit (STEMCELL TECHNOLOGIES). Subsequently, whole-transcriptome libraries were constructed and deep sequencing was performed with the assistance of Novogene Co., Ltd. (Beijing). To analyze differential expression between the two groups, the DESeq2 R package was used. The Benjamini and Hochberg method was applied to adjust the generated p-values to control for the false discovery rate (FDR). Genes with an adjusted p-value less than 0.05, as determined by DESeq2, were identified as differentially expressed genes (DEGs). The clusterProfiler GO enrichment analysis of the upregulated DEGs was performed. In this analysis, GO terms with a p-value less than 0.05 were considered significantly enriched. The enriched GO terms related to immune response regulation were visualized using the ggplot2 R package.

Histopathological Analysis

On the 15th day after B16-F10 tumor seeding, tumor tissues were collected from the transplant and analyzed by hematoxylin and eosin (H&E) staining. Hearts, livers, spleens, lungs, and kidneys were harvested from tumor-bearing mice and fixed in a 4% paraformaldehyde solution. The organs were embedded in paraffin, sectioned, and stained for H&E. The sections were examined with a ZEISS Axiolab 5 microscope.

Serum Biochemical Markers and Cytokines

On the 15th day after B16-F10 tumor seeding, serum was collected from tumor-bearing mice, and specific enzymes and metabolites, including creatine kinase (CK), creatine kinase MB (CK-MB), α-hydroxybutyrate dehydrogenase (α-HBD), alanine aminotransferase (ALT), aspartate aminotransferase (AST), UREA, uric acid (UA), and creatinine (CREA) were detected using a specific kit from BeijingBJ.XinChuangYuan Biotech Co., Ltd. (Beijing) using an automatic biochemical analyzer Toshiba TBA-120FR (Japan). Cytokines were detected using the CBA Mouse Th1/Th2/Th17 Cytokine Kit via flow cytometric analysis according to the manufacturer's instructions.

Statistical Analysis

The results were expressed as mean ± standard deviation (SD) or mean ± standard error of the mean (SEM). Statistical analyses were performed using the GraphPad Prism software (version 5.0). Differences between two groups were tested using an unpaired two-tailed Student's *t*-test. Differences among multiple groups were tested using two-way ANOVA,

followed by Tukey's multiple comparison test. The significance threshold was set at $p < 0.05$, with the exact p-values reported; $p \geq 0.05$ was considered not statistically significant (ns).

Results

Generation and Characterization of the Chimeric HBc VLP Nanovaccines

The nanovaccine-generation process is illustrated in Figure 1A. To co-deliver the tumor antigen and target TAMs, we engineered a chimeric HBc VLP by inserting MAGE-$A10_{254\text{-}262}$ into the MIR and fusing M2pep to the N-terminus of a C-terminally truncated HBc (1–149 aa) (Figure 1B). HBc-M2pep-$VLP_{MAGE\text{-}A10}$ (VLP) was expressed in *E. coli* BL21 (DE3) as inclusion bodies (Figure 1C, lane 4), purified by Ni-affinity chromatography (Figure 1D, peak 2), and confirmed as a 23-kDa monomer by SDS-PAGE and WB (Figure 1E and F, lane 1 and lane 2). The purified protein self-assembled into spherical VLP (Ø≈30 nm, TEM; Figure 1G) with a hydrodynamic diameter of 34.25±2.43 nm (PDI: 0.276±0.010) and zeta potential of −9.04±0.58 mV. Post-CpG encapsulation (CpG@VLP), the diameter increased to 35.45±1.07 nm and zeta potential of −10.07 ± 0.09 mV. To augment tumor targeting, αB7-H3 was conjugated to CpG@VLP via chemical crosslinking to generating CpG@VLP-αB7-H3 (Figure 1H). The unconjugated species were removed by size-exclusion chromatography (Figure 1I). Flow cytometry validated specific binding of CpG@VLP-αB7-H3 to B16-F10 cells via αB7-H3 (Figure 1J). To enhance biostability, CpG@VLP-αB7-H3 was PEGylated with mPEG5k-ALD, yielding CpG@VLP-αB7-H3-PEG, which increased the hydrodynamic diameter to 64.34 ± 3.18 nm (PDI: 0.327 ± 0.028) while maintaining core morphology (Ø ≈30 nm; Figure 1K), confirming a hydrated PEG layer. Figure 1L and M present the size-distribution curves and zeta-potential values, respectively, which demonstrate that the nanoparticles are homogeneous and negatively charged. In vitro safety profiling revealed negligible cytotoxicity in RAW264.7 macrophages. After 24 h of incubation, the cell viability exceeded 80% at 50 μg/mL, although marginally elevated cytotoxicity was observed in the CpG@VLP group (Figure 1N).

M2pep Coupling to the VLP Nanovaccine Promotes TAM Targeting and PEGylation Attenuates Phagocytosis

To assess TAM targeting by the VLP nanovaccine, FITC-labeled VLP (FITC-VLP) was incubated with TAM-like macrophages derived from B16-F10 tumor medium-polarized RAW264.7 cells. After staining with anti-lysosome antibody and DAPI, confocal microscopy revealed enhanced intracellular green fluorescence in VLP-treated TAMs, whereas scrambled M2pep control VLP (scVLP) and PEGylated VLP (PEG-VLP) showed reduced signals (Figure 2A). To validate the findings in a primary cell model, FITC-VLP was incubated with primary TAMs derived from C57BL/6 mouse BMDMs. Flow cytometry demonstrated a 1.57-fold increase ($p < 0.0001$) in $FITC^+$ TAMs with VLP versus those with scVLP (Figure 2B). PEG-VLP reduced the fluorescence intensity by 27.5% ($p < 0.0001$) compared with unmodified VLP, indicating that PEGylation attenuates phagocytosis or protein adherence by macrophages. Qualitative and quantitative in vitro analyses showed that VLP displayed markedly greater binding to TAMs. Following in vitro validation, Cy5-labeled VLP (Cy5-VLP) were intravenously injected into B16-F10 tumor-bearing SCID mice. IVIS imaging (Figure 2C) and quantitative analysis (Figure 2D) revealed preferential tumor accumulation. At 30 min post-injection, tumor fluorescence intensity exceeded the levels in the major organs (heart, lung, spleen, kidney, and liver). Cryosectioned tumors stained with anti-F4/80 or anti-CD206 antibodies and DAPI showed colocalization of Cy5-VLP (red) with TAM markers (green) in confocal images (Figure 2E), indicating VLP accumulation within TAMs. Collectively, these findings demonstrate that VLP efficiently targets TAMs in vitro and in vivo, and that PEG modification decreases protein adherence or phagocytosis by macrophages, suggesting a prolonged circulation time in vivo.

CpG@VLP Efficiently Reprograms TAMs and αB7-H3 Conjugation Further Enhances T Cell Activation

As a TLR9 agonist, CpG has been reported to reprogram M2-like TAMs into an M1-like phenotype.[36] BMDMs from C57BL/6 mice were cultured with M-CSF and converted to TAMs using the B16-F10 tumor medium. M2-to-M1 phenotype reversion was analyzed using flow cytometry after treating TAMs with CpG, VLP, or CpG@VLP (Figure 3A shows representative plots; quantitative data in Figure 3B–D). Figure 3B presents the relative proportions of the polarization markers. Following treatment,

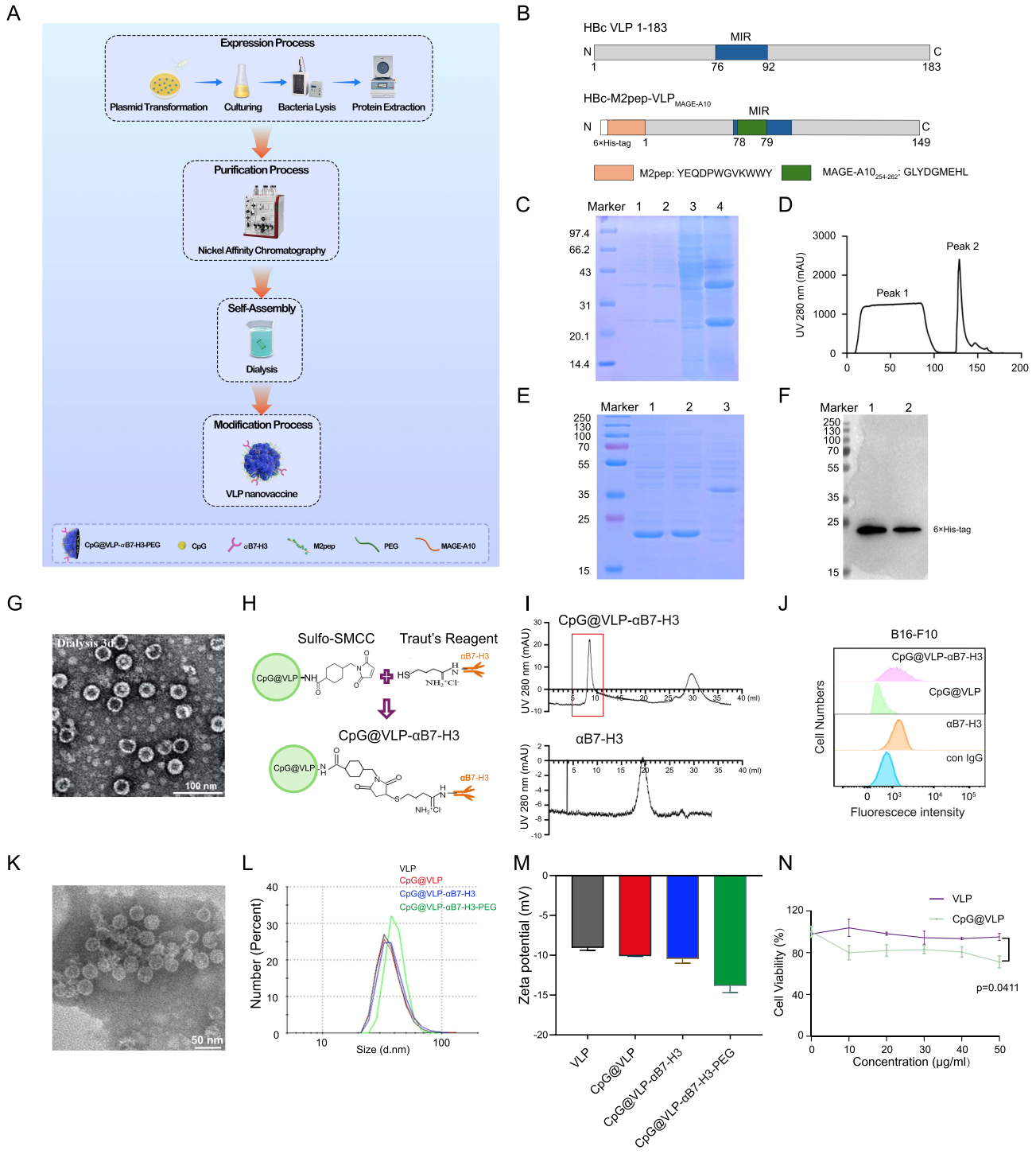

Figure 1 Generation and characterization of VLP nanovaccines. (**A**) Schematic illustration of the preparation steps of VLP nanovaccines. (**B**) Schematic diagram of HBc VLP and the chimeric protein based on it. (**C**) Inclusion bodies expression (Lane 1: pre-induction; Lane 2: IPTG post-induction; Lane 3: supernatant after sonication lysis; Lane 4: pellet fraction after sonication lysis), (**D**) Ni-affinity chromatography purification (Peak 1: flow-through during loading; Peak 2: target protein elution with 300 mM imidazole buffer), (**E**) SDS-PAGE (Lane1 and 2: protein after Nickel affinity chromatography purification; Lane3: fluid-through during Nickel affinity chromatography purification), and (**F**) Western blot detection (Lane1 and 2: protein after Nickel affinity chromatography purification) of VLP. (**G**) Representative microscopic morphology under transmission electron microscopy of VLP, scale bar = 100 nm. (**H**) Schematic diagram of generation of CpG@VLP-αB7-H3 by conjugation CpG@VLP with αB7-H3. (**I**) Conjugated CpG@VLP-αB7-H3 purification (up: red square) and control free αB7-H3 outflow (down) by size-exclusion chromatography. (**J**) Flow cytometry-based binding assay for CpG@VLP-αB7-H3 binding to B16-F10 cells via αB7-H3. (**K**) Representative microscopic morphology under transmission electron microscopy of CpG@VLP-αB7-H3-PEG, scale bar = 50 nm. Representative size distribution (**L**) and zeta potential (**M**) of VLP, CpG@VLP, CpG@VLP-αB7-H3 and CpG@VLP-αB7-H3-PEG. (**N**) Cytotoxicity assay of RAW264.7 cells incubated with VLP and CpG@VLP for 24 h by CCK-8 assay (n = 3, mean ± SD).

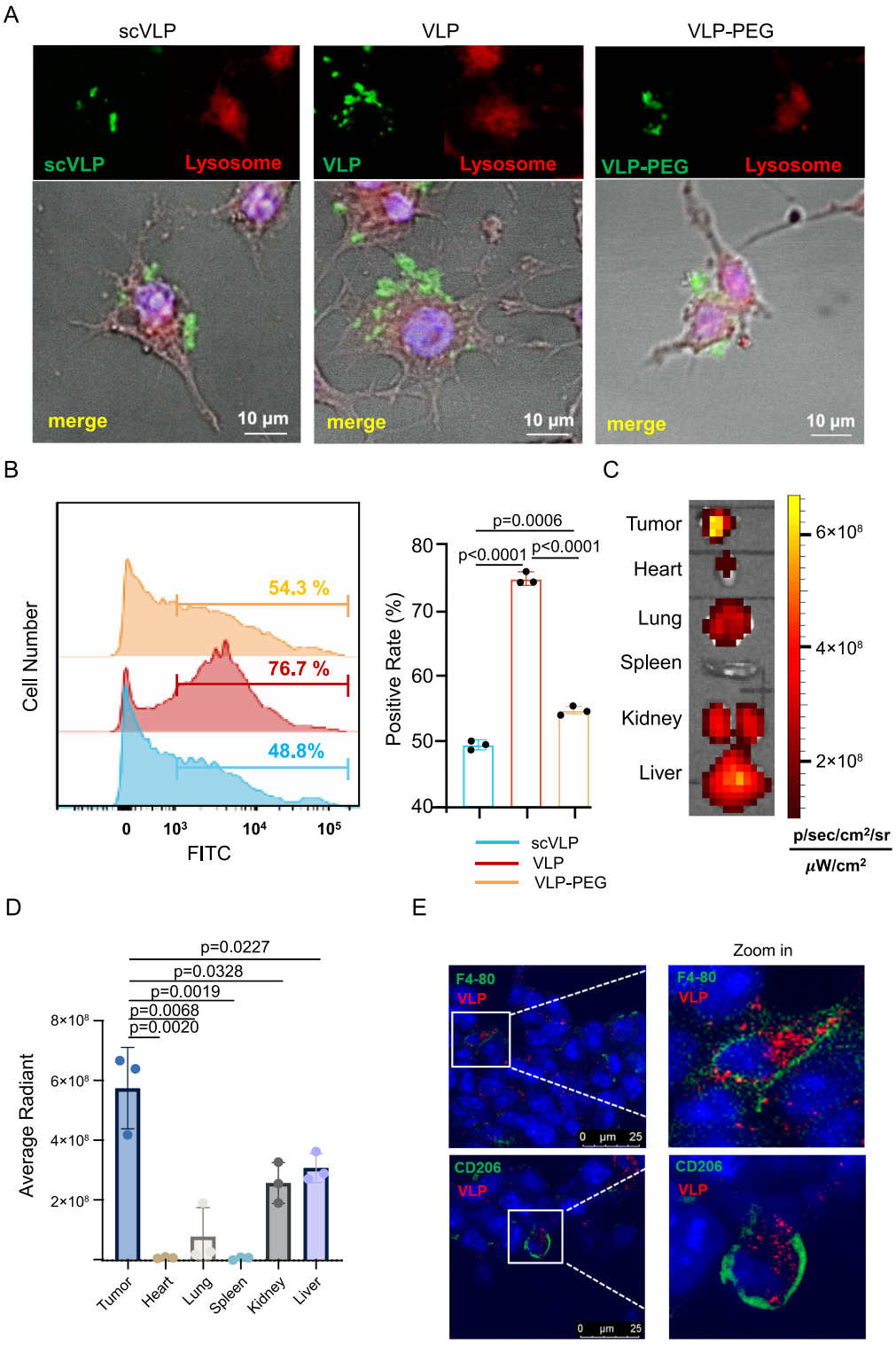

Figure 2 Targeting capability of VLP nanovaccines to TAMs in vitro and in vivo. (**A**) TAMs from B16-F10 tumor medium-pulsed RAW264.7 cells were incubated with FITC-labeled VLP nanovaccines at the concentration of 5 μg/mL for 4 h. The TAMs targeting capability of the VLP nanovaccines was imaged on a confocal microscope using the same settings (blue: DAPI; red: Lysosome; green: scVLP, VLP, or VLP-PEG), scale bar = 10 μm. (**B**) TAMs from B16-F10 tumor medium-pulsed BMDMs were incubated with FITC-labeled VLP nanovaccines at the concentration of 5 μg/mL for 4 h. The TAM targeting capability of the VLP nanovaccines was analyzed by Flow cytometry. (**C**) SCID mice bearing 2-week B16-F10 tumors (5 × 10^5 subcutaneous on Day 0) were injected via the tail vein with 100 μg of Cy5-labeled VLP. At 30 min, mice were sacrificed, and tumors and organs were harvested. Images were representative of three biological replicates. IVIS images of tumors and organs excised from mice injected with Cy5-labeled VLP were demonstrated. (**D**) Uptake of VLP by tumors compared with the heart, lung, spleen, kidney, and liver. (**E**) Tumors were cryosectioned, stained, and imaged on a confocal microscope using the same settings (blue: DAPI; red: VLP; green: F4/80, or CD206), scale bar = 25 μm. (n = 3, mean ± SD).

https://doi.org/10.2147/IJN.S548334

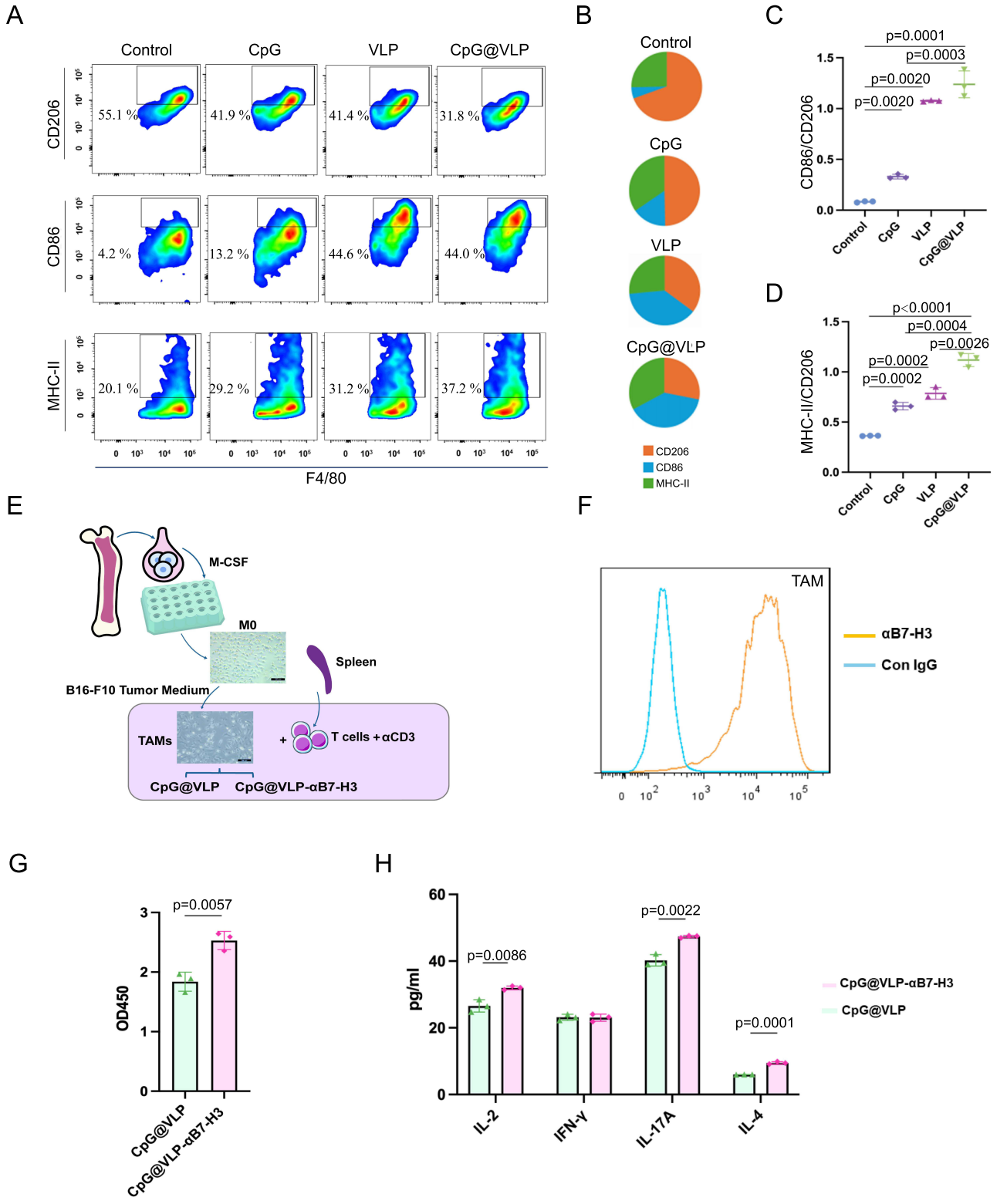

Figure 3 In vitro TAM phenotype reversion and T cell activation. (**A**) Representative dot plot of M2-like TAM surface marker CD206 together with M1-like TAM surface markers CD86 and MHC II on $CD11b^{+}F4/80^{+}$-gated TAMs was analyzed by flow cytometry after treatment with CpG or the VLP nanovaccines. (**B**) The relative proportion of polarization markers after treatment with CpG or the VLP nanovaccines was calculated. (**C** and **D**) The TAM phenotype reversion reflected by the M1/M2 ratio CD86/CD206 and MHC-II/CD206 after treatment with CpG or the VLP nanovaccines was calculated. (**E**) Experimental procedures for coculturing T cells purified from spleen of congenic C57BL/6 mouse with TAMs that have been treated using VLP nanovaccines. (**F**) Expression of B7-H3 on TAMs. (**G**) T cell proliferation after cocultured with nanovaccine-treated TAMs by CCK-8 assay. (**H**) T cell-related cytokines secretion after co-cultured with nanovaccine -treated TAMs by Cytometric Bead Array. (n = 3, mean ± SD).

CD206 (M2 marker) expression decreased, whereas CD86 and MHC-II (M1 markers) expression increased in $CD11b^+F4/80^+$ TAMs. To better quantify the phenotypic shift, CD86/CD206 and MHC-II/CD206 ratios were calculated as indicators of the M1/M2 polarization status. As shown in Figure 3C and D, the CpG@VLP group exhibited the most pronounced reversal in M1/M2 ratios. Specifically, ratios increased from 0.08 (control) to 1.24 (15.50-fold; $p = 0.0001$) for CD86/CD206, and from 0.36 to 1.12 (3.11-fold; $p < 0.0001$) for MHC-II/CD206. Therefore, CpG@VLP efficiently reprogrammed the M2-like TAMs to an M1-like phenotype. To further evaluate the efficacy of the reprogrammed TAMs in activating T cells, experiments were conducted, as outlined in Figure 3E. Mouse BMDMs were polarized into M2-like TAMs using the B16-F10 tumor medium. The induced TAMs were then treated with CpG@VLP or CpG@VLP-αB7-H3. Flow cytometry confirmed significant B7-H3 expression on the TAM surfaces (Figure 3F), validating the targetability of B7-H3. T cells isolated from syngeneic mouse spleens were co-cultured with treated TAMs at an 8:1 T cell-to-TAM ratio in the presence of anti-CD3 antibody (αCD3) to activate the TCR signaling pathway. After 72 h of co-culture, T cell proliferation was assessed using the CCK-8 assay. The results demonstrated that CpG@VLP-αB7-H3-treated TAMs enhanced T cell proliferation by 1.38-fold ($p = 0.0057$) compared with CpG@VLP-treated TAMs (Figure 3G). This indicates that αB7-H3 conjugation potentiates T cell activation in vitro. The levels of cytokines in the co-culture supernatants were quantified to further evaluate T cell activation (Figure 3H). Macrophages treated with CpG@VLP-αB7-H3 showed significantly increased secretion of T cell-associated cytokines compared to CpG@VLP-treated TAMs. Specifically, IL-2, IL-17A, and IL-4 production increased by 1.20-fold ($p = 0.0086$), 1.18-fold ($p = 0.0022$), and 1.57-fold ($p = 0.0001$), respectively. Collectively, CpG@VLP-αB7-H3 activated T cells more efficiently than CpG@VLP in vitro through B7-H3 blockade.

Tumor Growth Is Inhibited After Treatment with VLP Nanovaccines in vivo

To evaluate the in vivo antitumor capability of VLP-based nanovaccines, C57BL/6 mice were subcutaneously inoculated with B16-F10 tumor cells to generate a highly aggressive tumor model. Mice bearing tumors (~5 mm in diameter by day 7) were randomly assigned to groups and treated intratumorally (i.t.) or intraperitoneally (i.p.), as shown in Figure 4A. Administration of VLP nanovaccines significantly delayed tumor growth (Figure 4B). By Day 15, tumors were harvested and photographed for gross morphological assessment (Figure 4C). Compared with the PBS controls, all treatments resulted in significantly higher tumor inhibition rates (Figure 4D): αB7-H3 (25.25%, $p = 0.0359$), CpG@VLP (63.47%, $p < 0.0001$), CpG@VLP-αB7-H3 (68.15%, $p < 0.0001$), and CpG@VLP-αB7-H3-PEG (80.12%, $p < 0.0001$). Although CpG@VLP-αB7-H3 treatment did not yield a significantly higher tumor inhibition rate than CpG@VLP alone, possibly due to the low conjugated αB7-H3 dose (150 μg) or compensatory immune cell infiltration; CpG@VLP-αB7-H3-PEG, consistent with our hypothesis, showed the strongest effect, indicating PEG's role in sustained release. H&E staining revealed extensive necrosis and immune infiltration in nanovaccine-treated tumors (Figure 4E), suggesting that induced necrosis and immune cell recruitment may be linked, with infiltrating cells potentially contributing to the induction of necrosis.

VLP Nanovaccines Ameliorate the Tumor Immune Microenvironment in vivo

To further investigate the tumor immune microenvironment, single-cell suspensions from treated B16-F10 tumors were analyzed by flow cytometry (Figure S1A). Compared to the PBS control and αB7-H3 groups, the VLP-nanovaccine-treated groups showed significantly increased $CD45^+$ cells. Specifically, CpG@VLP-αB7-H3 increased $CD45^+$ cells by 7.17-fold compared with PBS ($p = 0.0002$), outperforming CpG@VLP (5.35-fold, $p = 0.0009$) (Figure 5A). Despite a 6.75-fold increase in $CD45^+$ increase in CpG@VLP-αB7-H3-PEG (vs 7.17-fold in CpG@VLP-αB7-H3), its optimal antitumor efficacy (80.12% inhibition, Figure 4D) suggests that PEG-mediated sustained immune stimulation outweighs the higher peak immune cell recruitment. TAM reprogramming toward a tumor-suppressive phenotype was observed; all nanovaccines significantly increased $iNOS^+$TAMs (Figure 5B), correlating with the tumor inhibition rate (eg, 63.47% for CpG@VLP; Figure 4D). Critically, αB7-H3 conjugation further boosted $iNOS^+$ TAMs ($p = 0.0009$ vs CpG@VLP), whereas all nanovaccines reduced $CD206^+$ M2 macrophages (Figure S1B), confirming M2-to-M1 repolarization. Synergistic T cell activation was detected: CpG@VLP-αB7-H3 enhanced $CD69^+$ expression in $CD4^+/CD8^+$ T cells (Figure 5C and D), and PEG further amplified $CD4^+$ T cell activation (not significantly). Mechanistically, CpG@VLP predominantly increased granzyme B in $CD8^+$ T cells (Figure 5E), whereas αB7-H3 specifically elevated perforin levels in $CD8^+$ T cells (Figure 5F), demonstrating complementary CTL enhancement mechanisms. RNA-seq analysis of $CD45^+$

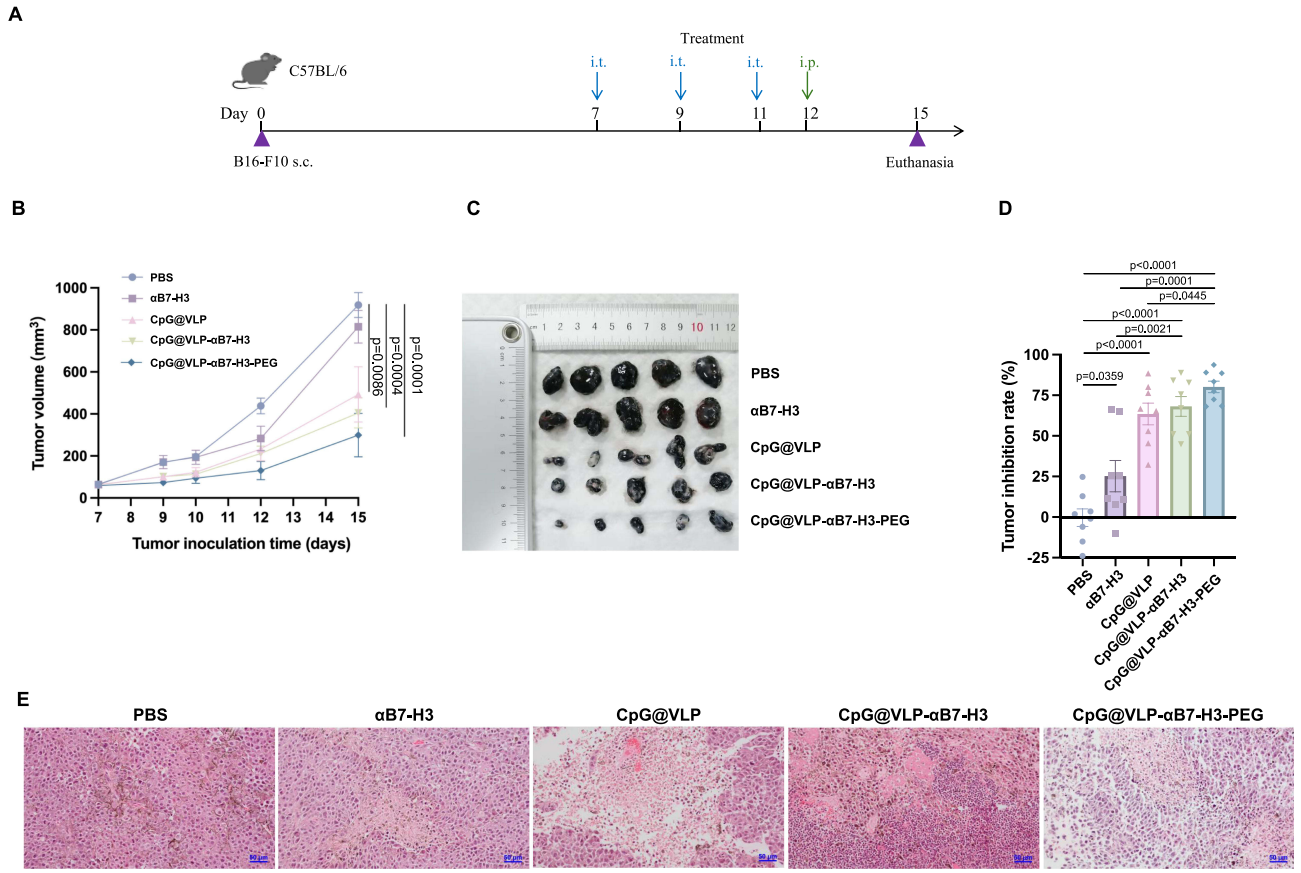

Figure 4 Antitumor effects after treatment with VLP nanovaccines in the B16-F10 tumor model. (**A**) Schemes of tumor inoculation and treatments. (**B**) Representative tumor volume growth curve from mice in each treatment group (n = 5, mean ± SEM). (**C**) Images of tumors on Day 15 harvested from mice in each treatment group. (**D**) Tumor volume inhibition rate after receiving various treatments was compared with mice treated with PBS (n = 8, mean ± SEM). (**E**) Representative evidence of necrosis in tumor site of each group by hematoxylin and eosin (H&E) staining, scale bar = 50 μm. Differences among multiple groups were tested with two-way ANOVA followed by Tukey's multiple comparison for tumor volume (**B**) and unpaired two-tailed Student's *t* test was used to compare means for tumor inhibition (**D**).

cell DEGs further confirmed immune remodeling. GO enrichment of upregulated DEGs in CpG@VLP-αB7-H3 vs PBS control revealed M1-like macrophage signatures (Figure 5G) and adaptive immune response pathways (Figure 5H). Additionally, DEGs in CpG@VLP-αB7-H3 vs CpG@VLP were enriched for positive regulation of cytokine production, leukocyte chemotaxis, and migration (Figure S1C). Collectively, nanovaccines remodel the tumor microenvironment by repolarizing TAMs to a tumor-suppressive phenotype and activating cytotoxic T-cell responses.

VLP Nanovaccines Improve Systemic Tumor Antigen-Specific Antitumor Immunity

Considering that antitumor immunity is dependent on tumor antigen-specific T cell responses, tumor antigens are crucial for the initiation of antitumor immunity. To evaluate systemic antitumor immunity, splenocytes from treated B16-F10-bearing mice were antigen-specifically restimulated with MAGE-A10-inserted VLP or co-cultured with B16-F10 tumor cells to assess their reactivity against native tumor antigens (Figure 6A). First, tumor antigen-specific T cell priming was observed. VLP restimulation induced significantly greater proliferation of antigen-specific T cells in splenocytes in all nanovaccine groups than in PBS ($p < 0.0001$, Figure 6B), peaking at 3.35-fold in CpG@VLP-αB7-H3-PEG ($p < 0.0001$ vs all groups). MAGE-A10 specificity confirmed that sustained antigen release enabled robust T cell expansion. Secondly, synergistic enhancement of T cell activation was detected (Figure 6C): αB7-H3/CpG@VLP monotherapy increased $CD69^+$ expression in $CD4^+$/$CD8^+$ T cells vs PBS ($p < 0.01$), αB7-H3 conjugation enhanced $CD4^+$ T cell activation vs CpG@VLP ($p = 0.01$), and PEGylation increased activation to 19.83-fold ($CD4^+$) and 12.90-fold ($CD8^+$) vs PBS ($p < 0.001$). Third, CTL effector function (Figure 6D): $CD107a^+$ degranulation on $CD8^+$ T cells was significantly increased in the CpG@VLP-αB7-H3 and CpG@VLP-αB7-H3-PEG groups vs PBS ($p < 0.01$). Moreover, cytokine

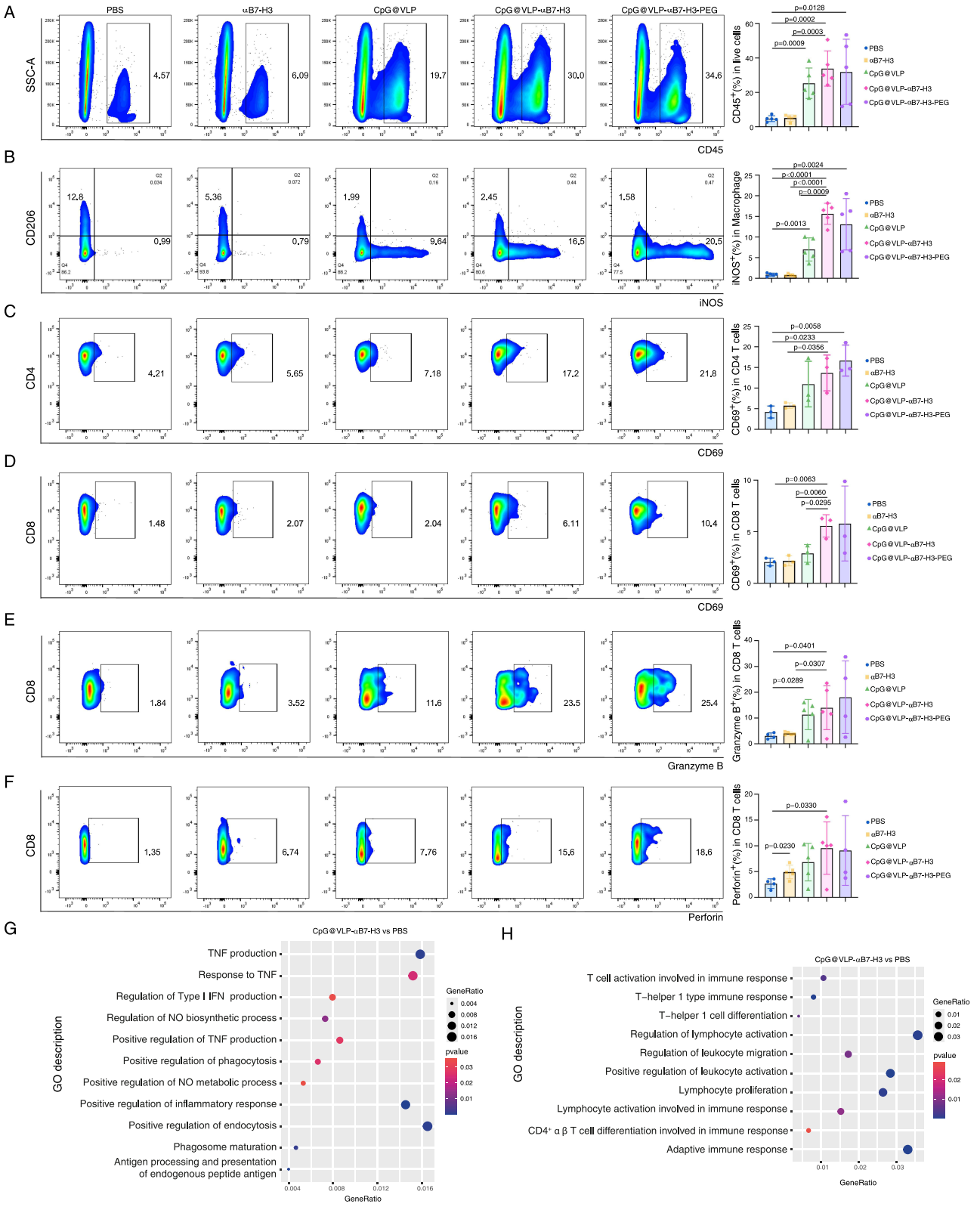

Figure 5 Tumor immune microenvironment remodeling after treatment with VLP nanovaccines in the B16-F10 tumor model. (**A**) $CD45^+$ cells, (**B**) $iNOS^+$ in macrophages ($CD45^+CD11b^+F4/80^+$), (**C**) $CD69^+$ in $CD4^+$ T cells ($CD45^+CD3^+CD4^+$), (**D**) $CD69^+$ in $CD8^+$ T cells ($CD45^+CD3^+CD8^+$), (**E**) Granzyme B^+ in $CD8^+$ T cells, and (**F**) Perforin$^+$ in $CD8^+$ T cells in tumor tissue of each treatment group ($n \geq 3$, mean ± SD). (**G** and **H**) GO enrichment scatter plot for up-regulated transcriptome genes for CpG@VLP-αB7-H3 compared with PBS in $CD45^+$ cells sorting from tumor tissue ($n = 3$), genes with an adjusted p value less than 0.05 were identified as differentially DEGs. For GO enrichment analysis of the upregulated DEGs, GO terms with a p value less than 0.05 were considered significantly enriched.

https://doi.org/10.2147/IJN.S548334

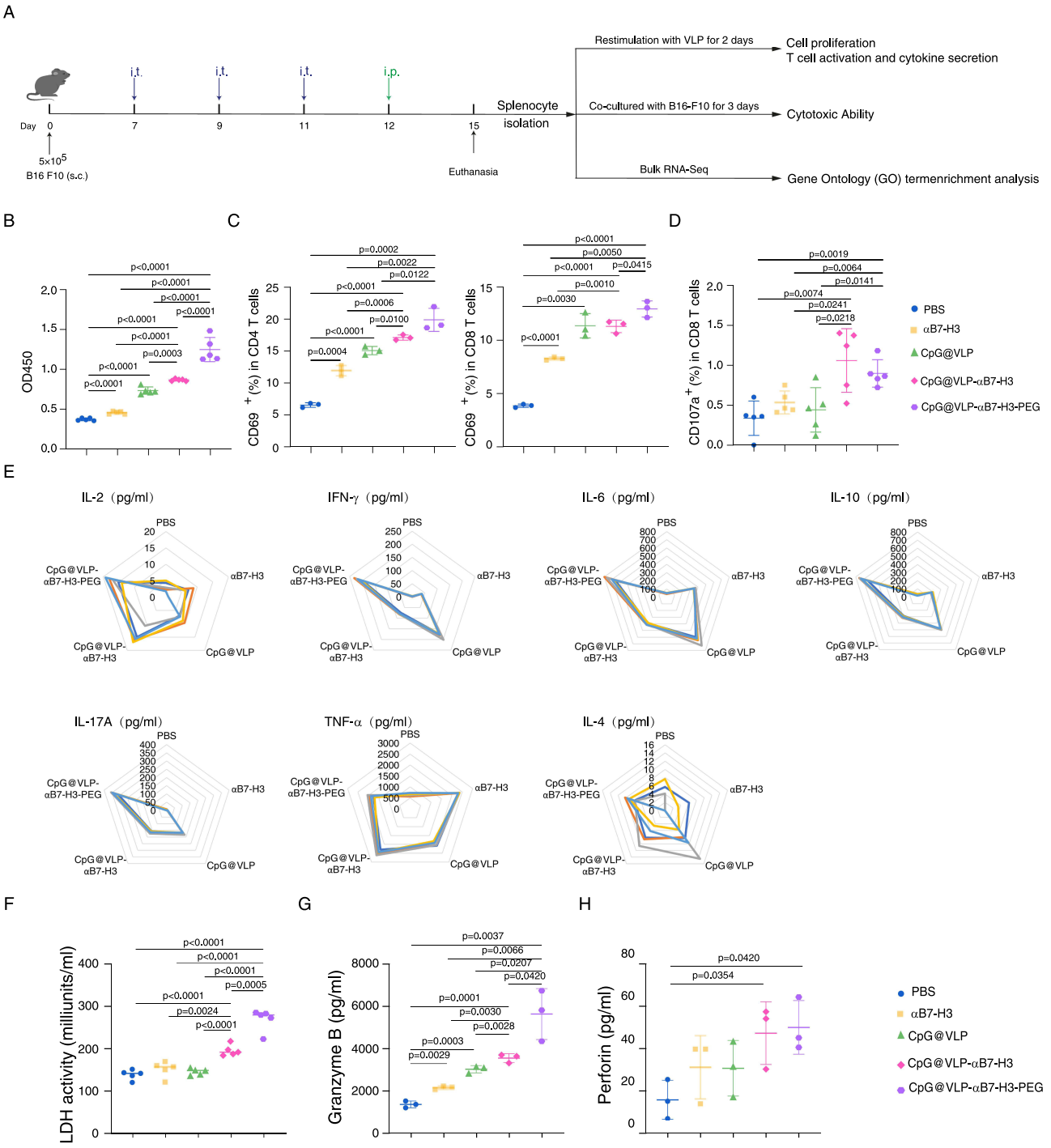

Figure 6 Improved systemic antitumor immunity from VLP nanovaccine-treated B16-F10 tumor-bearing mice. (**A**) Schemes of tumor inoculation, VLP nanovaccines administration, splenocyte isolation and treatment. (**B–E**) In vitro splenocytes were restimulated with 5 μg/mL of VLP for 48 h. (**B**) Cell proliferation was evaluated by CCK-8 kit. (**C**) The activation of T cell (% $CD69^+CD4^+$ T cell and % $CD69^+CD8^+$ T cell) and (**D**) cytotoxic T cells (% $CD107a^+CD8^+$ T cell) was measured by flow cytometry. (**E**) Cytokine secretion from culture supernatant was determined by Cytometric Bead Array Th1Th2Th17 kit. In vitro splenocytes were co-cultured with B16-F10 tumor cells for cytotoxic assay, including (**F**) LDH activity, (**G**) Granzyme B secretion, and (**H**) Perforin secretion using specific ELISA kit. (n ≥ 3, mean ± SD).

profiling showed: CpG@VLP-αB7-H3-PEG induced the maximal secretion of Th1 cytokines (IL-2 and IFN-γ), proinflammatory cytokines (IL-6 and IL-17A), and regulatory IL-10 (Figure 6E), suggesting potent cellular immunity alongside regulatory mechanisms. Importantly, functional tumor cell killing assays demonstrated that CpG@VLP-αB7-H3 markedly enhanced LDH (1.40-fold, $p < 0.0001$, Figure 6F) and perforin release (2.93-fold, $p = 0.0354$, Figure 6H)

compared to PBS. Granzyme B secretion (Figure 6G) was increased in αB7-H3/CpG@VLP monotherapy vs PBS ($p < 0.01$), was enhanced by αB7-H3 conjugation compared to CpG@VLP ($p = 0.0028$), and was amplified 4.02-fold by PEGylation vs PBS ($p = 0.042$ vs CpG@VLP-αB7-H3). Notably, CpG@VLP-αB7-H3-PEG exhibited maximal LDH/granzyme B ($p < 0.05$ vs all groups) and perforin ($p < 0.05$ vs PBS) levels, validating that PEGylation sustained antigen-specific killing.

Mechanism of VLP Nanovaccine-Enhanced Systemic Antitumor Immunity

To further elucidate the mechanism of sustained antitumor immunity in vivo, immunofluorescence was used to evaluate $CD8^+$ T cell-TAM interactions at tumor sites, while RNA-seq of splenocytes was used to analyze systemic immunity. Compared to the PBS control/αB7-H3-treated groups, the VLP nanovaccine groups showed significantly increased TAMs (green; Figure 7A), which was corroborated by GO analysis, revealing enhanced myeloid cell differentiation (Figure S2A). CpG@VLP-αB7-H3 induced a greater number of $CD8^+$ T cell (red)-TAM colocalization, with GO analysis confirming the enrichment of M1-like macrophage signatures (Figure S2B), T-cell activation pathways (Figure S2C), and leukocyte activation/immune response regulation (vs CpG@VLP; Figure S2D). Notably, CpG@VLP-αB7-H3-PEG exhibited peak $CD8^+$ T cell-TAM colocalization (correlating with 80.12% tumor inhibition; Figure 4D) and 148 upregulated DEGs (vs CpG@VLP-αB7-H3; Figure 7B) enriched in T cell activation and adaptive immune response (Figure 7C). Specifically, immune response activation (Figure 7D), T cell activation (Figure 7E), receptor-mediated endocytosis (Figure 7F), and the nitric oxide synthase biosynthetic process (Figure 7G). Collectively, αB7-H3 conjugation to CpG@VLP drives $CD8^+$ T-TAM colocalization, where reprogrammed TAMs provide a suitable APC niche for T cell activation and proliferation. PEGylation further reprograms M2-like TAMs into an M1-like phenotype and potentiates T cytotoxicity to enhance the systemic tumor antigen-specific antitumor immunity.

Evaluation of Toxicity of VLP Nanovaccine Treatment in vivo

The in vivo toxicity assessment of VLP nanovaccines revealed minimal adverse effects. Histological analysis (H&E staining) of the major organs (heart, liver, spleen, lung, and kidney) showed no obvious abnormalities (Figure 8A), indicating the absence of gross structural damage or inflammation at the tissue level. Furthermore, serum levels of key biochemical markers (Figure 8B), including cardiac markers (CK, CK-MB, and α-HBD), liver enzymes (ALT and AST), and renal function markers (UA, CREA, and UREA), remained within normal ranges or even showed signs of amelioration, potentially attributable to reduced tumor burden. These biochemical findings corroborate the histological results, providing strong evidence that nanovaccines caused no significant damage to the heart, liver, or kidney. Concurrently, serum cytokine profiling demonstrated a balanced Th1/Th2/Th17 response, specifically in the CpG@VLP-αB7-H3-PEG group versus CpG@VLP-αB7-H3 (Figure 8C), indicating that nanovaccine did not induce a harmful or dysregulated systemic immune response. This balanced cytokine profile is desirable for vaccines, because it reflects immune activation without overstimulation. Collectively, the normal tissue histology, absence of organ-specific serum biomarker elevation, and balanced cytokine profile strongly support that this novel multifunctional nanovaccine exhibits minimal in vivo toxicity. Crucially, this favorable safety profile was achieved along with efficient antitumor effects, which is a vital finding for the potential future translation of this nanovaccine platform.

Discussion

Accumulating evidence suggests that the TME plays a critical role in tumor progression and that TME regulators are promising cancer immunotherapeutic targets.[37,38] In the present study, a novel "all-in-one" nanovaccine, CpG@VLP-αB7-H3-PEG, was successfully developed to reprogram immunosuppressive TAMs and activate T-cells to target tumors. By exploiting the unique properties of HBc VLP, M2pep, MAGE-A10 peptide, CpG, αB7-H3, and PEG, our approach holds great promise for enhancing tumor immunotherapy and overcoming the challenges posed by the immunosuppressive tumor microenvironment. MAGE-$A10_{254\text{-}262}$ was incorporated into the MIR, and M2pep was incorporated into the N-terminus of HBc VLP via fusion expression. This design enables specific recognition and delivery of CpG to M2-like TAMs, facilitating their remodeling. Subsequently, αB7-H3 was loaded for the immune checkpoint blockade. The MAGE-$A10_{254\text{-}262}$ tumor-associated antigen peptide was presented to promote and activate antigen-specific $CD8^+$

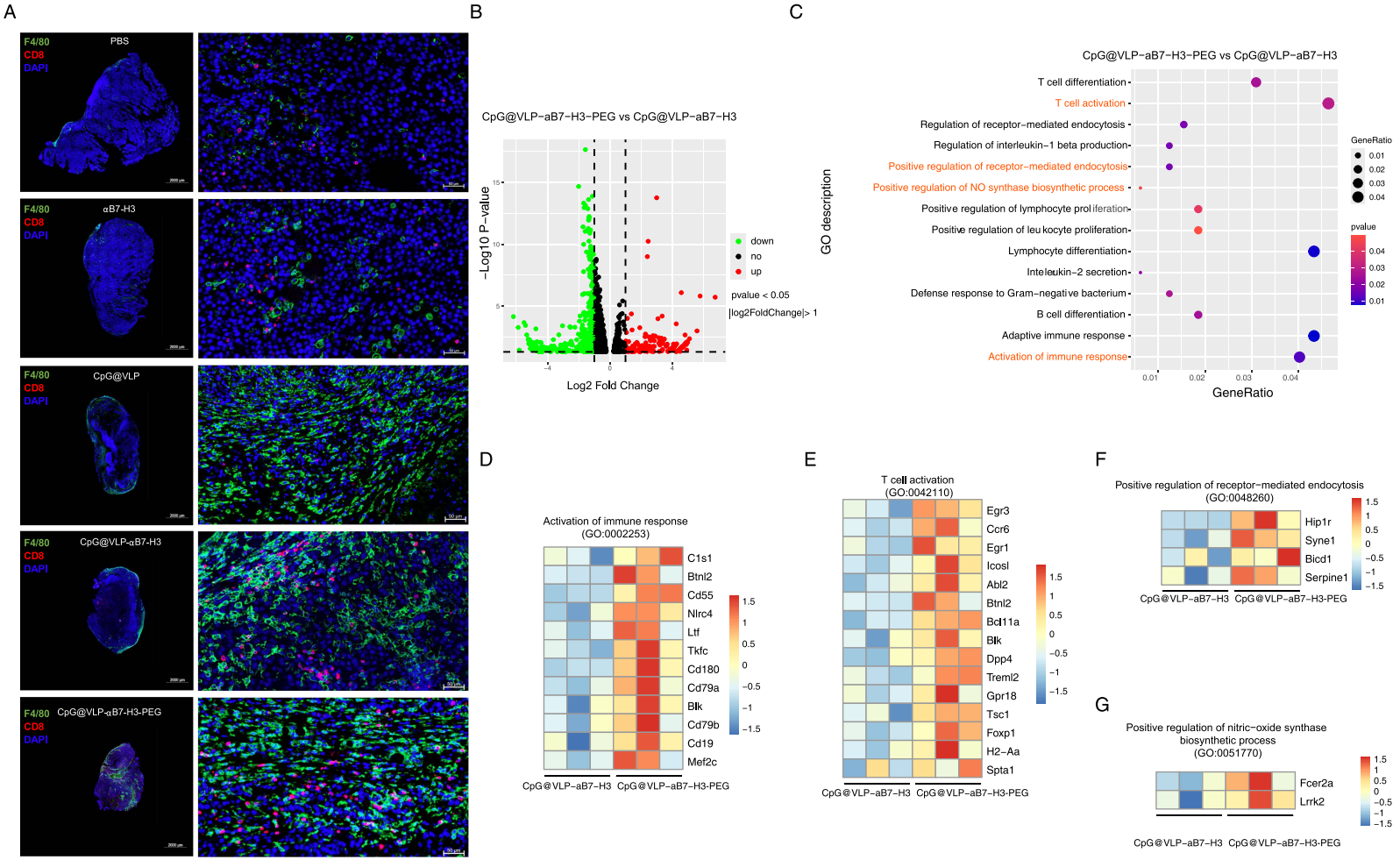

Figure 7 Mechanism for sustained system tumor antigen-specific antitumor immunity by CpG@VLP-αB7-H3-PEG. (**A**) Representative image of colocalization of TAMs (green-positive cells) with $CD8^+$ T cells (red-positive cells) in the tumor tissues by immunofluorescent assay (blue: DAPI; green: F4/80; red: CD8). Scale bars = 2000 μm for panoramic imaging (left) and 50 μm for zoom in image (right). (**B**) Volcano plots depict DEGs, (**C**) GO enrichment scatter plot for up-regulated DEGs from splenocyte of CpG@VLP-αB7-H3-PEG group (vs CpG@VLP-αB7-H3 group). (**D–G**) Heatmap of up-regulated DEGs, including (**D**) Activation of immune response, (**E**) T cell activation, (**F**) Positive regulation of receptor−mediated endocytosis, and (**G**) Positive regulation of nitric−oxide synthase biosynthetic process in CpG@VLP-αB7-H3-PEG group (vs CpG@VLP-αB7-H3). For (**B–G**) (n = 3), genes with an adjusted *p* value less than 0.05 were identified as DEGs. For GO enrichment analysis of the upregulated DEGs, GO terms with a *p* value less than 0.05 were considered significantly enriched.

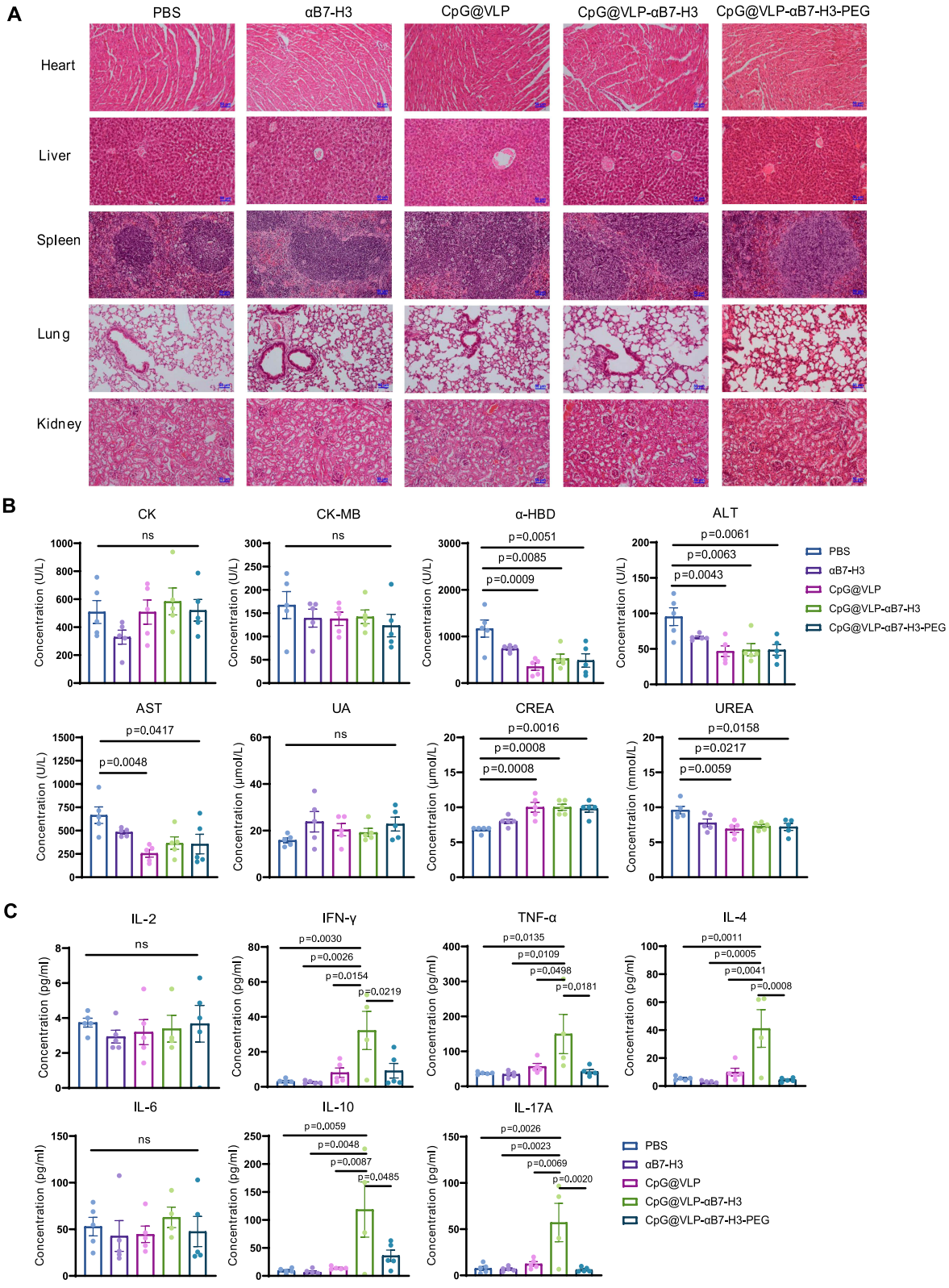

Figure 8 In vivo toxicity of VLP nanovaccines. (**A**) Representative H&E-stained slice images of major organs in each treatment group were demonstrated, scale bar = 50 μm. (**B**) Serum biochemical markers of CK, CK-MB, α-HBD, ALT, AST, UA, CREA, and UREA in each treatment group were measured with specific kit (n = 5, mean ± SD). (**C**) Serum cytokines of IL-2, IFN-γ, TNF-α, IL-4, IL-6, IL-10, and IL-17A in each treatment group was determined by Cytometric Bead Array Th1Th2Th17 kit (n ≥ 4, mean ± SD). Differences among multiple groups were tested with two-way ANOVA followed by Tukey's multiple comparison tests. *p* values less than 0.05 were considered significant, with the corresponding value number specified. p ≥ 0.05 was considered not statistically significant (ns).

https://doi.org/10.2147/IJN.S548334

T cells to achieve comprehensive cancer immunotherapy. Moreover, PEG was conjugated to the surface of CpG@VLP-αB7-H3, which decreased phagocytosis by macrophages and protein adhesion, thereby prolonging the relative retention time in the body. Therefore, nanoparticle accumulation at the tumor site increases, leading to enhanced efficacy of tumor immunotherapy.

In our study, PEGylation played a critical role in enhancing the therapeutic efficacy of nanovaccines. Compared to unmodified VLP, PEG-modified nanovaccines demonstrated decreased cellular uptake by TAMs in vitro (Figure 2A and B), which suggests that PEGylation improved the circulation time of the nanoparticles in vivo. This prolonged circulation ensures that the nanoparticles remain in the bloodstream longer, increasing their chances of reaching the tumor site to exert their therapeutic effects. This extended circulation time, combined with the tumor-homing properties of αB7-H3 modification, allows for increased accumulation of the nanovaccine in tumor tissues and improved interaction with TAMs, ultimately enhancing antitumor efficacy. Additionally, PEGylation likely contributed to a sustained-release property of the nanovaccines. The reduced engulfment of PEG-modified VLP by macrophages (Figure 2A and B) implies that the release of cargo (eg, CpG, αB7-H3) is slower and more prolonged,[39] potentially maintaining effective drug concentrations at the tumor site over time. This sustained release helps to sustainably activate immune cells and enhance antitumor immune responses.[40,41] Consistent with these properties, CpG@VLP-αB7-H3-PEG nanovaccines demonstrated the most potent antitumor activity in vivo, as evidenced by the strongest tumor growth inhibition (Figure 4B and D). Moreover, these nanovaccines significantly promoted splenocyte proliferation (Figure 6B), enhanced T-cell activation (Figure 6C), and stimulated cytokine secretion upon encountering VLP (Figure 6E) or B16-F10 tumor cells (Figure 6F–H). RNA-seq analysis further confirmed the upregulation of pathways related to nitric oxide synthase biosynthesis (Figure 7G), receptor-mediated endocytosis (Figure 7F), T-cell activation (Figure 7E), and adaptive immune response (Figure 7D). These findings suggest that PEGylation not only enhances the physical properties of the nanovaccines but also positively regulates the tumor immune microenvironment. This dual role likely contributes to the activation of the body's antitumor immune response and ultimately improves therapeutic efficacy.

Although M2pep was originally discovered in mouse systems,[42] recent studies have demonstrated its selective binding to M2-like macrophages in both murine and human models, with minimal interaction with M1-like macrophages.[34] This cross-species activity suggests that M2pep has the potential to target human TAMs effectively. Furthermore, the development of a subtype-specific probe, M2pep-uIONP, for targeted magnetic resonance imaging of M2-like TAMs in glioblastoma, using an orthotopic patient-tissue-derived xenograft (PDX) mouse model, provides additional evidence of its translational potential.[43] However, we acknowledge that several challenges need to be addressed before this strategy can be translated to clinical settings. First, further validation in more diverse human models and clinical samples is required to confirm the specificity and affinity of M2pep for human TAMs. Second, the stability and biodistribution of M2pep-based probes in humans need to be optimized to ensure effective targeting and minimal off-tissue accumulation. Finally, the safety and immunogenicity of M2pep in humans must be thoroughly evaluated in preclinical studies before advancing to clinical trials. M2pep plays a crucial role in the present strategy owing to its high affinity for M2-like TAMs, enabling selective binding and internalization, which ensures targeted delivery of therapeutics.[44] In the present study, VLP displayed greater uptake by M2-like TAMs than scVLP. Furthermore, the passive enhanced permeability and retention (EPR) effect promotes the selective distribution of nanoparticles in tumor tissues, increases drug efficacy, and reduces systemic side effects.[45] Consistently, a greater number of VLP accumulated in tumor tissues than in important organs, as evidenced by quantitative in vivo imaging in the present study. Thus, the development of M2pep-modified VLP may provide a promising strategy for effectively targeting M2-like TAMs and TME.

CpG has been well documented for its ability to convert M2-like TAMs to the M1-like phenotype, thereby augmenting the antitumor immune response.[36] However, the in vivo instability and poor cellular uptake of CpG, owing to nuclease degradation, pose significant limitations. To overcome these issues, nanomaterials such as VLP have been employed as carriers to increase their delivery to APCs and improve tumor antigen presentation.[46] In the present study, VLP loaded with CpG effectively induced a phenotypic shift into M1-like macrophages in vitro, as demonstrated by the increased CD86 and MHC II expression and decreased CD206 expression. Interestingly, VLP alone was found to shift the macrophage M1/M2 balance toward the M1 phenotype. This observation is consistent with previous studies showing that hepatitis B core antigen impairs the polarization of M2-like macrophages while promoting the production of inflammatory cytokines via the TLR2 pathway.[47] CpG@VLP-treated mice exhibited approximately 63.47% tumor growth inhibition in vivo, which was accompanied by increased infiltration of $CD45^+$ cells in the tumor tissue. Specifically, the increased presence of $iNOS^+$ macrophages

and granzyme B^+CD8^+ T cells, along with decreased $CD206^+$ macrophages, indicates the successful reprogramming of M2-like TAMs to M1-like macrophages. These reprogrammed TAMs function as APCs, presenting MAGE-A10 antigen to $CD8^+$ T cells and promoting their proliferation and cytotoxicity. Splenocyte proliferation assays further confirmed tumor antigen-specific activation, as evidenced by CD69 expansion on $CD4^+$ T cells and $CD8^+$ T cells upon restimulation with MAGE-$A10_{254\text{-}262}$-modified VLP.

B7-H3 is an important immune checkpoint in cancer, and B7-H3 expression frequently correlates with decreased tumor-infiltrating lymphocytes, accelerated cancer progression, and worse clinical outcomes, making it an attractive and promising target for cancer immunotherapy.[6–9,48] In the present study, the conjugation of αB7-H3 to CpG@VLP effectively blocked B7-H3 on macrophages, thereby relieving the inhibitory effect on T cells. This leads to enhanced T-cell proliferation and increased secretion of IL-2, IL-17A, and IL-4 in vitro. However, the CCK-8 assay, while useful for assessing metabolic activity, has limitations in directly reflecting T cell proliferation. Future studies should employ multiple complementary methods to more accurately evaluate both viability and proliferation of T cells. CpG@VLP-αB7-H3 treatment in vivo resulted in increased infiltration of $CD69^+CD4^+$ T cells and $CD69^+CD8^+$ T cells, and expanded populations of granzyme B^+CD8^+ T cells and perforin$^+CD8^+$ T cells in tumor tissues. The αB7-H3-driven perforin elevation aligns with B7-H3's role in regulating cytolytic activity, whereas CpG@VLP predominantly increased granzyme B, which underscores TLR9-mediated CTL priming. This functional specialization underlies the superior antitumor efficacy of nanovaccines. Moreover, compared with those in the CpG@VLP group, the number of $iNOS^+$ macrophages was greater in tumor tissues from the CpG@VLP-αB7-H3 group. These results demonstrated that the addition of the blocking anti-B7-H3 antibody to the CpG@VLP platform significantly enhanced the antitumor immune response by increasing the number of infiltrating immune cells and the proportion of functional CTLs in tumor tissues.

In summary, the novel engineered CpG@VLP-αB7-H3-PEG nanovaccine demonstrated significant antitumor efficacy in B16-F10 melanoma-bearing mice. Further studies in various cancer models with specific tumor antigens loaded with blocking antibodies or immune adjuvants could be implemented on the VLP platform for precise medical strategies. However, several aspects require further investigation before they can be translated into clinical applications. First, although M2pep shows promise for targeting mouse M2-like macrophages, the differences in gene expression between human and mouse macrophages necessitate the identification of specific ligands that target human M2-like macrophages. Further identification of ligands that target human M2-like macrophages is required for translation of this platform into human clinical trials. Second, the present expression system using engineered *Escherichia coli* BL21 (DE3) with inclusion body purification needs to be optimized. To accelerate clinical translation, a scale-up process, establishment of quality control standards for VLP content, and improvements in drug loading efficiency in GMP production departments are essential. Future studies should explore eukaryotic expression systems for more efficient VLP purification from soluble supernatants. Furthermore, while our current study focuses on TAMs and $CD4^+$/$CD8^+$ T cells, memory T cells and NK cells—both critical for durable anti-tumor immunity—should be examined in future work.

Conclusion

In conclusion, the novel multifunctional CpG@VLP-αB7-H3-PEG nanovaccine based on HBc VLP represents a promising universal strategy for personalized cancer immunotherapy by reprogramming immunosuppressive TAMs and activating T-cells. Continued research in this direction is expected to accelerate the development of effective cancer treatments.

Ethics

All experimental procedures involving animals were performed by the Institutional Animal Care and Use Committee of Beijing Shijitan Hospital, Capital Medical University (KYD-2024-0049-001). All procedures complied with the relevant guidelines and regulations. Animal welfare and experimental procedures complied with the principles of the Laboratory Animal Guidelines for the Ethical Review of Animal Welfare (GB/T 35892-2018).

Acknowledgments

This study was financially supported by the R&D Program of the Beijing Municipal Education Commission (Grant No. KZ202110025028), the Chinese Institutes for Medical Research, Beijing (Grant No. CX24PY28), the National Natural

Science Foundation of China (Grant Nos. 82171814, 81973262, and 82011530138), the Beijing Natural Science Foundation (Grant No. L248068), Independent Research Project of the China Academy of Chinese Medical Sciences (No.YZ-202117), and Industrial Science and Technology Program in Taizhou (23gya01).

Disclosure

The authors report no potential conflicts of interest in this work.

References

1. Bray F, Laversanne M, Sung H, et al. Global cancer statistics 2022: GLOBOCAN estimates of incidence and mortality worldwide for 36 cancers in 185 countries. *CA Cancer J Clin*. 2024;74(3):229–263. doi:10.3322/caac.21834
2. Dagher OK, Schwab RD, Brookens SK, Posey AD. Advances in cancer immunotherapies. *Cell*. 2023;186(8):1814. doi:10.1016/j.cell.2023.02.039
3. Lv M, Chen M, Zhang R, et al. Manganese is critical for antitumor immune responses via cGAS-STING and improves the efficacy of clinical immunotherapy. *Cell Res*. 2020;30(11):966–979. doi:10.1038/s41422-020-00395-4
4. Katz MHG, Petroni GR, Bauer T, et al. Multicenter randomized controlled trial of neoadjuvant chemoradiotherapy alone or in combination with pembrolizumab in patients with resectable or borderline resectable pancreatic adenocarcinoma. *J Immunother Cancer*. 2023;11(12):e007586. doi:10.1136/jitc-2023-007586
5. Stromnes IM, Hulbert A, Rollins MR, et al. Insufficiency of compound immune checkpoint blockade to overcome engineered T cell exhaustion in pancreatic cancer. *J Immunother Cancer*. 2022;10(2): e003525.
6. Getu AA, Tigabu A, Zhou M, et al. New frontiers in immune checkpoint B7-H3 (CD276) research and drug development. *Mol Cancer*. 2023;22 (1):43. doi:10.1186/s12943-023-01751-9
7. Zhao B, Li H, Xia Y, et al. Immune checkpoint of B7-H3 in cancer: from immunology to clinical immunotherapy. *J Hematol Oncol*. 2022;15 (1):153. doi:10.1186/s13045-022-01364-7
8. Luan S, Zhao Y, Yu Y, et al. B7-H3 The relevance of B7-H3 and tumor-associated macrophages in the tumor immune microenvironment of solid tumors: recent advances. *Am J Transl Res*. 2025;17(4):2835–2849. doi:10.62347/ILTR3848
9. Cheng M, Chen S, Li K, et al. CD276-dependent efferocytosis by tumor-associated macrophages promotes immune evasion in bladder cancer. *Nat Commun*. 2024;15(1):2818. doi:10.1038/s41467-024-46735-5
10. Liu J, Yang S, Cao B, et al. Targeting B7-H3 via chimeric antigen receptor T cells and bispecific killer cell engagers augments antitumor response of cytotoxic lymphocytes. *J Hematol Oncol*. 2021;14(1):21. doi:10.1186/s13045-020-01024-8
11. Dai X, Cao B, Liu X, et al. Tumor vascular normalization by B7-H3 blockade augments T lymphocyte-mediated antitumor immunity. *Eur J Pharmacol*. 2025;993:177334. doi:10.1016/j.ejphar.2025.177334
12. Gao Y, Wang X, Zhang C, et al. Tumor immunotherapy targeting B7-H3: from mechanisms to clinical applications. *Immunotargets Ther*. 2025;14:291–320. doi:10.2147/ITT.S507522
13. O'Connell BC, Hubbard C, Zizlsperger N, et al. Eganelisib combined with immune checkpoint inhibitor therapy and chemotherapy in frontline metastatic triple-negative breast cancer triggers macrophage reprogramming, immune activation and extracellular matrix reorganization in the tumor microenvironment. *J Immunother Cancer*. 2024;12(8):e009160.
14. He L, Tam PKH, Deng CX. Orchestration of tumor-associated macrophages in the tumor Cell-Macrophage-CD8 + T cell loop for cancer immunotherapy. *Int J Bio Sci*. 2025;21(9):4098–4116. doi:10.7150/ijbs.115932
15. Nian Z, Dou Y, Shen Y, et al. Interleukin-34-orchestrated tumor-associated macrophage reprogramming is required for tumor immune escape driven by p53 inactivation. *Immunity*. 2024;57(10):2344–2361. doi:10.1016/j.immuni.2024.08.015
16. Zhang A, Xu Y, Xu H, et al. Lactate-induced M2 polarization of tumor-associated macrophages promotes the invasion of pituitary adenoma by secreting CCL17. *Theranostics*. 2021;11(8):3839–3852. doi:10.7150/thno.53749
17. Wang S, Wang J, Chen Z, et al. Targeting M2-like tumor-associated macrophages is a potential therapeutic approach to overcome antitumor drug resistance. *NPJ Precis Oncol* 2024. 8(1): 31.
18. Cao Y, Qiao B, Chen Q, et al. Tumor microenvironment remodeling via targeted depletion of M2-like tumor-associated macrophages for cancer immunotherapy. *Acta Biomater*. 2023;160:239–251. doi:10.1016/j.actbio.2023.02.006
19. Zhang XZ, Wei Z, Yong T, et al. Cell microparticles loaded with tumor antigen and resiquimod reprogram tumor-associated macrophages and promote stem-like CD8+ T cells to boost anti-PD-1 therapy. *Nat Commun*. 2023;14(1):5653. doi:10.1038/s41467-023-41438-9
20. Goswami S, Anandhan S, Raychaudhuri D, Sharma P. Myeloid cell-targeted therapies for solid tumours. *Nat Rev Immunl*. 2023;23(2):106–120. doi:10.1038/s41577-022-00737-w
21. Liu Z, Li S, Xiao Y, et al. A Multi-Functional nanoadjuvant coupling manganese with toll-like 9 agonist stimulates potent innate and adaptive antitumor immunity. *Adv Sci*. 2024;11(41):e2402678. doi:10.1002/advs.202402678
22. Zeng YC, Young OJ, Wintersinger CM, et al. Fine tuning of CpG spatial distribution with DNA origami for improved cancer vaccination. *Nat Nanotechnol*. 2024;19(7): 1055–1065.
23. Wei J, Wu D, Shao Y, et al. ApoE-mediated systemic nanodelivery of granzyme B and CpG for enhanced glioma immunotherapy. *J Control Release*. 2022;347:68–77. doi:10.1016/j.jconrel.2022.04.048
24. Ruzzi F, Semprini MS, Scalambra L, et al. Virus-like particle (VLP) vaccines for cancer immunotherapy. *Int J Mol Sci*. 2023;24(16):12963. doi:10.3390/ijms241612963
25. Li W, Jing Z, Wang S, et al. P22 virus-like particles as an effective antigen delivery nanoplatform for cancer immunotherapy. *Biomaterials*. 2021;271:120726. doi:10.1016/j.biomaterials.2021.120726
26. Kant R, Lee L-S, Patterson A, et al. Small molecule assembly agonist alters the dynamics of hepatitis B virus core protein dimer and capsid. *J Am Chem Soc*. 2024;146(42):28856–28865. doi:10.1021/jacs.4c08871
27. Cheng K, Ma N, Liang J, et al. Site-specific modification of virus-like particles for exogenous tumor Antigen display and minimizing preexisting immunity. *Small*. 2023;19(23):e2300125. doi:10.1002/smll.202300125

28. Kheirvari M, Liu H, Tumban E. Virus-like particle vaccines and platforms for vaccine development. *Viruses*. 2023;15(5):1109. doi:10.3390/v15051109
29. McCright J, Skeen C, Yarmovsky J, Maisel K. Nanoparticles with dense poly(ethylene glycol) coatings with near neutral charge are maximally transported across lymphatics and to the lymph nodes. *Acta Biomater*. 2022;145:146–158. doi:10.1016/j.actbio.2022.03.054
30. Awaad A, Takemoto H, Iizuka M, et al. Changeable net charge on nanoparticles facilitates intratumor accumulation and penetration. *J Control Release*. 2022;346:392–404. doi:10.1016/j.jconrel.2022.04.025
31. Poojary M, Jishnu PV, Kabekkodu SP. Prognostic value of melanoma-associated antigen-A (MAGE-A) gene expression in various human cancers: a systematic review and meta-analysis of 7428 patients and 44 studies. *Mol Diagn Ther*. 2020;24(5):537–555. doi:10.1007/s40291-020-00476-5
32. Kerkar SP, Wang Z-F, Lasota J, et al. MAGE-A is more highly expressed than NY-ESO-1 in a systematic immunohistochemical analysis of 3668 cases. *J Immunother*. 2016;39(4):181–187. doi:10.1097/CJI.0000000000000119
33. Hussain T, Zhao Z, Murphy B, et al. Chemically tagging cargo for specific packaging inside and on the surface of virus-like particles. *ACS Nano*. 2024;18(32):21024–21037. doi:10.1021/acsnano.4c02056
34. Chen Y, Gong L, Cao Y, et al. Reprogramming tumor-associated macrophages by a dually targeted milk exosome system as a potent monotherapy for cancer. *J Control Release*. 2024;366:395–409. doi:10.1016/j.jconrel.2023.12.058
35. Blumenschein GR, Devarakonda S, Johnson M, et al. Phase I clinical trial evaluating the safety and efficacy of ADP-A2M10 SPEAR T cells in patients with MAGE-A10 + advanced non-small cell lung cancer. *J Immunother Cancer*. 2022;10(1):e003581. doi:10.1136/jitc-2021-003581
36. Han S, Wang W, Wang S, et al. Tumor microenvironment remodeling and tumor therapy based on M2-like tumor associated macrophage-targeting nano-complexes. *Theranostics*. 2021;11(6):2892–2916. doi:10.7150/thno.50928
37. Cai Z, Li W, Hager S, et al. Targeting PHGDH reverses the immunosuppressive phenotype of tumor-associated macrophages through α-ketoglutarate and mTORC1 signaling. *Cell Mol Immunol*. 2024;21(5):448–465. doi:10.1038/s41423-024-01134-0
38. Xu X, Li T, Yang T, et al. A photoactivatable self-Assembled nanoagonist for synergistic therapy against pancreatic ductal adenocarcinoma. *Nano Lett*. 2024;24(39):12239–12248. doi:10.1021/acs.nanolett.4c02959
39. Sakurai Y, Yoshikawa K, Arai K, et al. siRNA delivery to lymphatic endothelial cells via ApoE-mediated uptake by lipid nanoparticles. *J Control Release*. 2023;353:125–133. doi:10.1016/j.jconrel.2022.11.036
40. Liang S, Chen Y, Zhang S, et al. RhB-encapsulating silica nanoparticles modified with PEG impact the vascular endothelial function in endothelial cells and zebrafish model. *Sci Total Environ*. 2020;711:134493. doi:10.1016/j.scitotenv.2019.134493
41. Wan S, Zhang B, Li S, et al. Combination of PEG-decorated black phosphorus nanosheets and immunoadjuvant for photoimmunotherapy of melanoma. *J Mater Chem B*. 2020;8(14):2805–2813. doi:10.1039/D0TB00434K
42. Cieslewicz M, Tang J, Yu JL, et al. Targeted delivery of proapoptotic peptides to tumor-associated macrophages improves survival. *PNAS*. 2013;110(40):15919–15924. doi:10.1073/pnas.1312197110
43. Li Y, Thamizhchelvan AM, Ma H, et al. A subtype specific probe for targeted magnetic resonance imaging of M2 tumor-associated macrophages in brain tumors. *Acta Biomater*. 2025;194:336–351.
44. Yang M, Wang B, Yin Y, et al. PTN-PTPRZ1 signaling axis blocking mediates tumor microenvironment remodeling for enhanced glioblastoma treatment. *J Control Release*. 2023;353:63–76. doi:10.1016/j.jconrel.2022.11.025
45. Chen X, Huang Y, Chen H, et al. Augmented EPR effect post IRFA to enhance the therapeutic efficacy of arsenic loaded ZIF-8 nanoparticles on residual HCC progression. *J Nanobiotechnology*. 2022;20(1):34. doi:10.1186/s12951-021-01161-3
46. Nagaoka M, Liao W, Kusamori K, Nishikawa M. Targeted delivery of immunostimulatory CpG oligodeoxynucleotides to antigen-presenting cells in draining lymph nodes by stearic acid modification and nanostructurization. *Int J Mol Sci*. 2022;23(3):1350. doi:10.3390/ijms23031350
47. Yi H, Zhang Y, Yang X, et al. Hepatitis B core antigen impairs the polarization while promoting the production of inflammatory cytokines of M2 macrophages via the TLR2 pathway. *Front Immunol*. 2020;11:535. doi:10.3389/fimmu.2020.00535
48. Liu H, Du H, Khabibullin D, et al. mTORC1 upregulates B7-H3/CD276 to inhibit antitumor T cells and drive tumor immune evasion. *Nat Commun*. 2023;14(1):1214. doi:10.1038/s41467-023-36881-7